An accurate strategy for computing reaction forces and fluxes on trimmed locally-refined meshes

Davide D'Angella*[1], Stefan Kollmannsberger[1], Alessandro Reali[2], Ernst Rank[1], and Thomas J.R. Hughes[3]

[1] *Chair of Computational Modeling and Simulation, Technische Universität München, Germany*
[2] *Department of Civil Engineering and Architecture, Università di Pavia, Italy*
[3] *Oden Institute for Computational Engineering and Sciences, The University of Texas at Austin, USA*

December 21, 2021

Abstract

The finite element method is classically based on nodal Lagrange basis functions defined on conforming meshes. In this context, total reaction forces are commonly computed from the so-called "nodal forces", yielding higher accuracy and convergence rates than reactions obtained from the differentiated primal solution ("direct" method). The finite cell method (FCM) and isogeometric analysis (IGA) promise to improve the interoperability of computer-aided design (CAD) and computer-aided engineering (CAE), enabling a direct approach to the numerical simulation of trimmed geometries. However, body-unfitted meshes preclude the use of classic nodal reaction algorithms.
This work shows that the direct method can perform particularly poorly for immersed methods. Instead, conservative reactions can be obtained from equilibrium expressions given by the weak problem formulation, yielding superior accuracy and convergence rates typical of nodal reactions. This approach is also extended to non-interpolatory basis functions, such as the (truncated) hierarchical B-splines.

1 Introduction

In many applications, the goal of finite-element analyses is to approximate specific physical quantities of interest. These data are often derived from the primal solution, such as in the case of total reaction forces or fluxes. Such quantities are often the most relevant data in engineering design and analysis.

The evaluation of fluxes and forces derived from the primal finite-element solution has been investigated for conforming meshes in several literature contributions. For example, in Akira [1986]; Barrett and Elliott [1987]; Brezzi et al. [2001]; Carey [1982]; Carey et al. [1985]; Gresho et al. [1987]; Hughes et al. [1987]; Hughes [2000]; Hughes et al. [2000]; Oshima et al. [1998] the flux is obtained through a modified variational problem with an additional auxiliary field corresponding to the normal flux over the Dirichlet boundary. Such an approach amounts to a mere post-processing step, and the resulting flux fulfills equilibrium in a global or local sense. This technique, referred to as conservative or consistent, is proven in the above references to be more accurate and achieve higher convergence orders than the "direct" approach of differentiating the primal solution. In Melbø and Kvamsdal [2003], reactions on mesh boundaries (subject to strong boundary conditions) are obtained for the Stokes flow through a variational

*davide.dangella@tum.de, Corresponding Author

interpretation similar to the one discussed in this work. In van Brummelen et al. [2011], similar formulas for the reactions on (conforming) mesh boundaries are studied, focusing on coupled problems. In the mentioned publications, the reactions are computed on Dirichlet-boundaries of meshes conforming to the computational domain. In Bazilevs and Hughes [2007], this approach is extended to computing reactions on (conforming) mesh boundaries subject to weak boundary conditions. In Bazilevs et al. [2012]; Kamensky et al. [2017]; Kamensky [2016]; Wu et al. [2017], consistent forces on immersed boundaries are considered on the fluid–structure coupling interface based on an augmented Lagrangian formulation.

In this work, the conservative reactions are first reviewed for conforming meshes subject to strong Dirichlet boundary conditions. This approach is then extended to non-conforming trimmed meshes, where the boundary of the geometry does not match the element boundaries. In particular, the total reaction flux is computed on boundaries subject to weak boundary conditions, such as the penalty [Babuška, 1973] and the symmetric Nitsche's [Nitsche, 1971] methods. The computation of the total fluxes for conforming meshes is viewed as testing a variational form with specific test functions, serving as "extraction functions" in the framework of Babuška and Miller [1984]. Namely, the reactions are obtained by the expression of equilibrium given by the weak form, yielding a total flux in global equilibrium with the other fluxes and data of the problem. Reactions are observed to converge with rates two times higher than the energy-norm error for Nitsche's method on a trimmed two-dimensional benchmark problem with a smooth solution. This phenomenon is often referred to as superconvergence [Babuška and Miller, 1984; Hughes et al., 2000; Szabó and Babuška, 2011; Wahlbin, 1995]. The same convergence rates are obtained for the penalty method, provided that the penalization parameter is suitably scaled.

Moreover, it is shown how this approach can be generalized to bases that do not form a partition of unity and are not based on the concept of "nodes". For example, this approach is valid for hierarchical B-splines ($\mathcal{HB}$) [Forsey and Bartels, 1988; Vuong et al., 2011], one promising approach to local refinement for isogeometric analysis [Hughes et al., 2005].

The structure of the paper is as follows. Section 2 motivates the conservative approach for computing the reactions. A three-dimensional trimmed example with a complex geometry defined by a Standard Triangle Language (STL) file is considered, showing that the direct method can perform particularly poorly for immersed meshes, as the weak boundary conditions indirectly constrain also the gradient of the solution. Section 6 explains how the standard way to compute the reactions can be interpreted as testing a variational form with specific test functions. This point of view serves as a basis to compute conservative reactions on trimmed bases not forming a partition of unity in Sections 7 and 8. In Section 9, it is shown that the method is superconvergent and approximates the total flux in a smooth two-dimensional problem with higher accuracy for both penalty and Nitsche's methods. In Section 10, the method is shown to give consistent results for both penalty and Nitsche's methods in the considered three-dimensional trimmed example. Finally, Section 11 shows how this approach can be applied to compute reaction tractions for isogeometric analysis of trimmed Kirchhoff-Love shells.

2 Motivation

Consider the portion of the façade element [Mungenast, 2017b] shown in Figure 1a. Its design takes advantage of the production freedom offered by additive manufacturing technologies to combine the aesthetics of wavy surfaces with functionalities such as insulation, ventilation, load transfer, and shading (cf. Mungenast [2017a,b]). These functionalities lead to a geometry featuring a complex internal structure and detailed external surfaces (cf. Figure 1b). The geometry is described by a fine STL file (courtesy of Dr. Moritz Mungenast), as displayed in Figure 1c. Note that the STL file does not define a computational geometry directly suitable for traditional methods based on conforming meshes.

The objective is to compute the total heat flux across the structure induced by a temperature difference

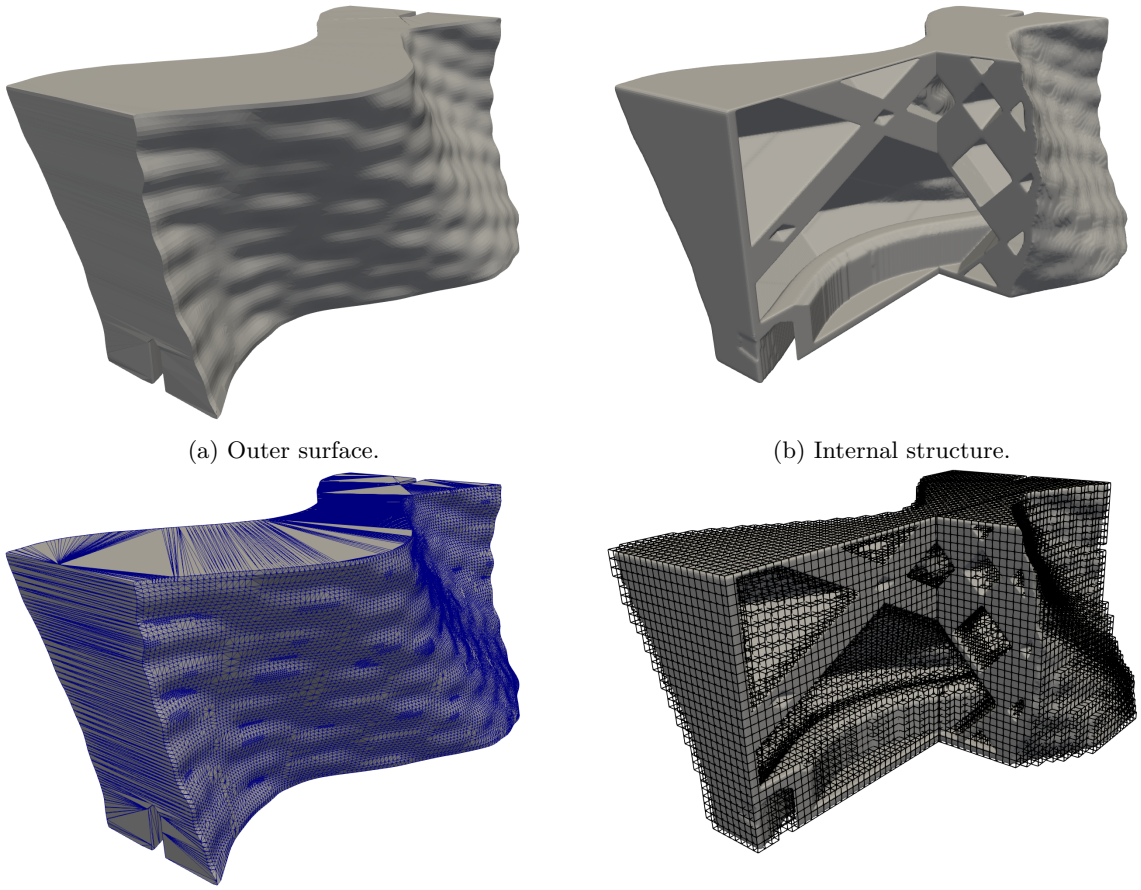

(a) Outer surface.

(b) Internal structure.

(c) STL file describing the geometry.

(d) Non-conforming computational mesh.

Figure 1: Portion of façade element [Mungenast, 2017b].

on two opposite faces. The following Laplace's equation and boundary conditions serve as a model problem

$$-\nabla \cdot (\boldsymbol{\kappa} \nabla u) = 0 \qquad \text{in } \Omega, \tag{1}$$

$$u = 0 \qquad \text{on } \Gamma_0, \tag{2}$$

$$u = 1 \qquad \text{on } \Gamma_1, \tag{3}$$

$$\boldsymbol{\kappa} \nabla u \cdot \boldsymbol{n} = 0 \qquad \text{on } \partial\Omega \setminus \overline{(\Gamma_0 \cup \Gamma_1)}. \tag{4}$$

Here, $\Omega \subset \mathbb{R}^3$ denotes the domain defined by the façade element, $\Gamma_0 \subset \partial\Omega$, and $\Gamma_1 \subset \partial\Omega$, $\Gamma_0 \cap \Gamma_1 = \emptyset$, denote the left and right boundaries highlighted in Figure 2a, $\boldsymbol{\kappa} \in \mathbb{R}^{3\times3}$ denotes the conductivity tensor, and $\boldsymbol{n}$ the outward unit boundary normal. Following the finite cell approach [Düster et al., 2017; Parvizian et al., 2007; Schillinger et al., 2012a], a simulation model is constructed without the need to build a conforming mesh, a potentially time-consuming step in the total simulation pipeline [Cottrell et al., 2009; Hughes et al., 2005]. The geometry Ω is immersed in a larger rectangular cuboid Ω^{fict} that can be straightforwardly meshed by a Cartesian element grid. As approximation, trivariate B-splines are used, rendering the immersed approach a trimmed trivariate Isogeometric Analysis. Figure 1d shows an example of elements intersecting the physical domain Ω. Since the boundaries Γ_0 and Γ_1, in general, do not coincide with a subset of element faces, but they are immersed in the elements, a strong imposition of the temperature boundary conditions would significantly deteriorate the accuracy. Instead, these boundary conditions are imposed weakly (cf., e.g., Ruess et al. [2013]; Schillinger et al. [2012b]), as explained in detail in Section 5. Figures 2b and 2c show the temperature and heat flux obtained with B-spline basis functions of order $p = 2$ and $\boldsymbol{\kappa}$ being the identity matrix. The boundary conditions are applied using Nitsche's method with stabilization parameter $\gamma = 10(p+1)^2/h$ (cf. Equation (17) and

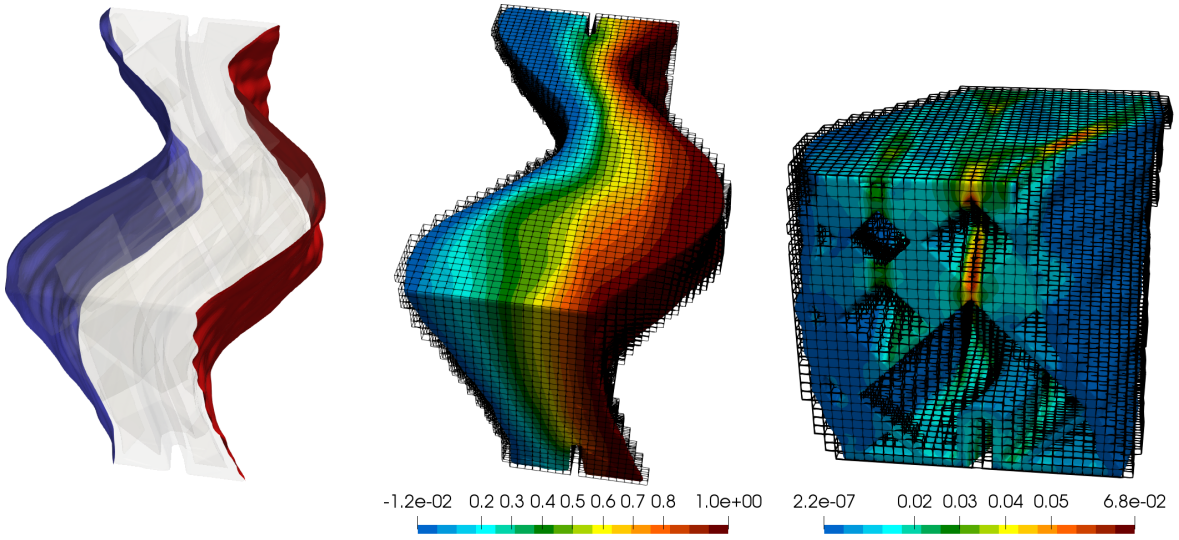

(a) Boundary conditions: $u = 0$ on the blue surface (Γ_0) and $u = 1$ on the red surface (Γ_1).

(b) Temperature.

(c) Heat-flux magnitude on the cross-section.

Figure 2: Boundary conditions and solution example for the façade element.

Antolin et al. [2019]; Johansson et al. [2019]), where h denotes the mesh size, as explained in Section 5.

A question now arises about the way to accurately compute the total flux from the trimmed discrete solution. Once a numerical solution u^h for the problem of Equations (1)–(4) is obtained, the conventional way for conforming finite elements with Lagrange shape functions and subject to strong boundary conditions can be summarized as in Table 1. It is yet not immediately clear how this conventional procedure

Let $\eta(\Gamma_0)$ be the set of nodes on Γ_0.

1. For each node $A \in \eta(\Gamma_0)$ associated with the nodal shape function N_A, compute the internal nodal flux
$$q_A = \int_\Omega \nabla N_A \cdot \left(\boldsymbol{\kappa} \nabla u^h\right) \, \mathrm{d}\Omega,$$
and the external nodal flux
$$q_A^e = \int_\Omega N_A f \, \mathrm{d}\Omega + \int_{\Gamma_h} N_A h \, \mathrm{d}\Gamma.$$
2. The reaction r on Γ_0 is obtained by summing the nodal fluxes of all nodes located on Γ_0, minus the known external fluxes
$$r = \sum_{A \in \eta(\Gamma_0)} q_A - q_A^e.$$

Table 1: The traditional algorithm for computing the reactions on conforming meshes of nodal partition-of-unity finite elements [Bathe, 2007; De Borst et al., 2012; Hughes, 2000; Hughes et al., 2000; Kohnke, 2009; Siemens PLM Software Inc, 2014].

can be used for trimmed meshes with non-nodal shape functions, as there are no nodes and the boundary is immersed in the element domains.

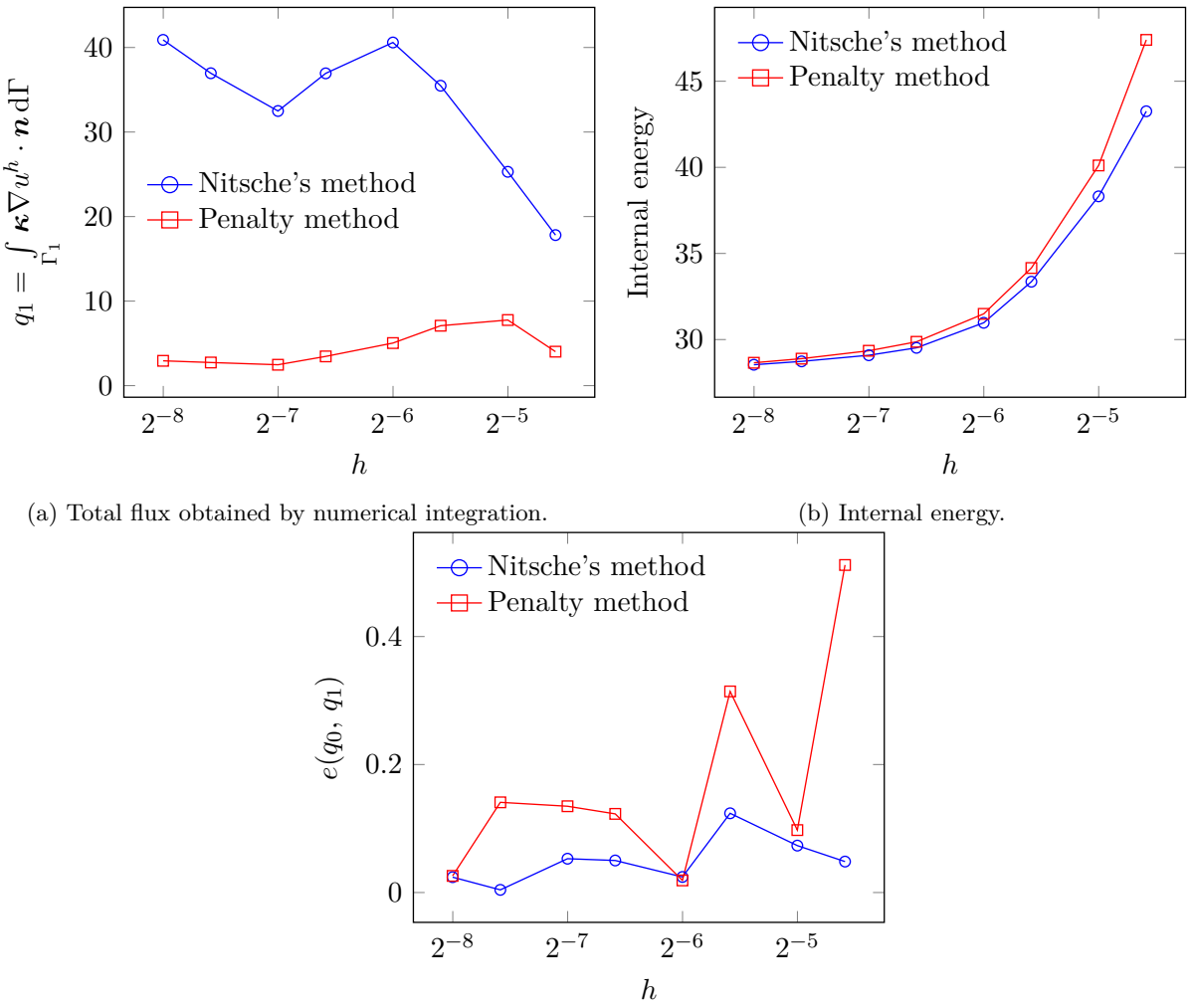

(a) Total flux obtained by numerical integration.

(b) Internal energy.

(c) Equilibrium error (cf. Equation (5)).

Figure 3: Flux across the Dirichlet boundary Γ_1, internal energy, and equilibrium for a sequence of bisected meshes.

Since the numerical solution u^h defines a numerical flux $\boldsymbol{\kappa}\nabla u^h$ for every spatial location $\boldsymbol{x} \in \Omega$ (u^h is assumed to be at least continuous), it is, in principle, possible to integrate numerically $\boldsymbol{\kappa}\nabla u^h \cdot \boldsymbol{n}$ over Γ_1. However, total fluxes computed in this way can have poor accuracy. Figure 3a shows that different total fluxes are obtained for Nitsche's method with stabilization parameter $\gamma = 10(p+1)^2/h$ (cf. Equation (17) and Antolin et al. [2019]; Johansson et al. [2019]) and the penalty method with penalization parameter $\beta = 10^2/h^p$ (cf. Equation (15)), where h denotes the mesh size, as explained in Section 5. Although the two methods yield different total fluxes, Figure 3b shows that the internal energy converges to the same value.

Moreover, if the numerical flux is integrated over Γ_0 and Γ_1, the obtained values are similar but not in perfect equilibrium. Such a difference is displayed in Figure 3c, where the relative error between the two fluxes is computed as

$$e(q_0^h, q_1^h) = \left| 1 - \frac{q_0^h}{-q_1^h} \right|, \tag{5}$$

where q_0^h and q_1^h represent the integrated flux $\boldsymbol{\kappa}\nabla u^h \cdot \boldsymbol{n}$ defined by the numerical solution u^h over Γ_0 and

Γ_1, respectively. Namely,

$$q_i^h = \int_{\Gamma_i} \boldsymbol{\kappa} \nabla u^h \cdot \boldsymbol{n} \, \mathrm{d}\Gamma, \qquad i \in \{0, 1\}. \tag{6}$$

This example indicates that integrating the numerical flux does not use all information contained in the finite element solution. Indeed, the underlying variational principle finds a solution that fulfills equilibrium in a global and local (element) sense [Bathe, 2007; Hughes et al., 2000]. Therefore, this information is contained in the solution. The rest of the paper is devoted to the development of a strategy to accurately extract it.

To this end, the article lays out an explanation for computing the total flux and reaction forces based on equilibrium considerations, generalizing the traditional approach to

- non-nodal basis functions that do not necessarily form a partition of unity,
- trimmed meshes.

Moreover, the proposed approach seems robust concerning the different methods for imposing the weak boundary conditions, in the sense that penalty and Nitsche's methods will converge to the same total-flux value.

3 The strong form of the model problem

Let $\Omega \subset \mathbb{R}^D$ be a bounded Lipschitz domain with disjoint Dirichlet and Neumann boundaries Γ_g, Γ_h, respectively, such that $\overline{\Gamma_g \cup \Gamma_h} = \partial\Omega$, $\Gamma_g \cap \Gamma_h = \emptyset$. The strong form of the heat conduction problem reads

$$-\nabla \cdot (\boldsymbol{\kappa} \nabla u) = f \qquad \text{in } \Omega, \tag{7}$$

$$u = g \qquad \text{on } \Gamma_g, \tag{8}$$

$$\boldsymbol{\kappa} \nabla u \cdot \boldsymbol{n} = h \qquad \text{on } \Gamma_h, \tag{9}$$

where $\boldsymbol{\kappa} \in \mathbb{R}^{D \times D}$ is the thermal-conductivity tensor, $h : \Gamma_h \to \mathbb{R}$ is the prescribed flux, $g : \Gamma_g \to \mathbb{R}$ is the prescribed temperature, $f : \Omega \to \mathbb{R}$ is the volumetric heat supply, and $\boldsymbol{n} \in \mathbb{R}^D$ is the vector normal to the boundary.

4 The weak form for strong boundary conditions

Given the set of trial functions $\mathcal{S}_{g,\Gamma_g}(\Omega)$ and the test space $\mathcal{W}_{0,\Gamma_g}(\Omega)$,

$$\mathcal{S}_{g,\Gamma_g}(\Omega) = \{u \in \mathcal{H}^1(\Omega) \,|\, u = g \text{ on } \Gamma_g\}, \tag{10}$$

$$\mathcal{W}_{0,\Gamma_g}(\Omega) = \{w \in \mathcal{H}^1(\Omega) \,|\, w = 0 \text{ on } \Gamma_g\}, \tag{11}$$

the weak form of the problem reads

$$\begin{aligned} &\text{find } u \in \mathcal{S}_{g,\Gamma_g}(\Omega) \\ &\text{such that } a(w, u) = l(w) \qquad \forall w \in \mathcal{W}_{0,\Gamma_g}(\Omega). \end{aligned} \tag{W}$$

Here, $a(w, u)$ and $l(w)$ denote the classic bilinear and linear forms

$$a(w, u) = (\nabla w, \boldsymbol{\kappa} \nabla u)_\Omega, \tag{12}$$

$$l(w) = (w, f)_\Omega + (w, h)_{\Gamma_h}, \tag{13}$$

4.1 The Galerkin form

Problem (W) can be rewritten with homogeneous Dirichlet boundary conditions by lifting g to Ω. In particular, let $g_\Omega \in \mathcal{H}^1(\Omega)$ be such that $g_\Omega|_{\Gamma_g} = g$. Then, $u_0 = u - g_\Omega$ belongs to $\mathcal{W}_{0,\Gamma_g}(\Omega)$ and Problem (W) can be stated as

$$\begin{aligned} &\text{find } u_0 \in \mathcal{W}_{0,\Gamma_g}(\Omega) \\ &\text{such that } a(w,\, u_0) = l(w) - a(w,\, g_\Omega) \qquad \forall w \in \mathcal{W}_{0,\Gamma_g}(\Omega). \end{aligned}$$

The Galerkin form of Problem (W) with a finite-dimensional subspace $\mathcal{W}^h_{0,\Gamma_g}(\Omega) \subset \mathcal{W}_{0,\Gamma_g}(\Omega)$ and an approximation g^h to g_Ω reads

$$\begin{aligned} &\text{find } u^h \in \mathcal{W}^h_{0,\Gamma_g}(\Omega) \subset \mathcal{W}_{0,\Gamma_g}(\Omega), \\ &\text{such that } a(w^h,\, u^h) = l(w^h) - a(w^h,\, g^h), \qquad \forall w^h \in \mathcal{W}^h_{0,\Gamma_g}(\Omega). \end{aligned} \tag{G}$$

5 The weak form for weak boundary conditions

In case the temperature boundary conditions are applied weakly, these are not incorporated in the solution and test spaces. Instead, an additional term $a_w(\cdot,\, \cdot)$ associated with the energy of the constraint violation is added as follows

$$\begin{aligned} &\text{find } u \in \mathcal{H}^1(\Omega) \\ &\text{such that } a(w,\, u) + a_w(w,\, u) = l(w) \qquad \forall w \in \mathcal{H}^1(\Omega). \end{aligned} \tag{w}$$

The term $a_w(w,\, u)$ can assume different forms depending on the weak-boundary approach. For the penalty method [Babuška, 1973] with a penalty parameter $\beta \in \mathbb{R}$, $a_w(w,\, u) = a_\beta(w,\, u)$ will be defined as

$$a_\beta(w,\, u) = (w,\, \beta(u - g))_{\Gamma_{\tilde{g}}}. \tag{14}$$

Typically, when using finite-element shape functions of polynomial order p, β is a mesh-dependent parameter scaled with h^p to retain the expected convergence rates [Utku and Carey, 1982]

$$\beta = \bar{\beta}\frac{1}{h^p}, \tag{15}$$

where $\bar{\beta} \in \mathbb{R}$ is a user-specified parameter, often dependent on the material parameters.

For the symmetric Nitsche's method [Nitsche, 1971] with stabilization parameter $\gamma \in \mathbb{R}$, $a_w(w,\, u) = a_\gamma(w,\, u)$ is defined as

$$a_\gamma(w,\, u) = -(\boldsymbol{\kappa}\nabla w \cdot \boldsymbol{n},\, u - g)_{\Gamma_g} - (w, \boldsymbol{\kappa}\nabla u \cdot \boldsymbol{n})_{\Gamma_g} + (w,\, \gamma(u - \tilde{g}))_{\Gamma_g}. \tag{16}$$

In this work, γ is scaled as in the original publication Nitsche [1971]

$$\gamma = \bar{\gamma}\frac{1}{h}. \tag{17}$$

For immersed methods, better estimates for γ can be obtained by solving a global or element-local generalized eigenvalue problem (cf., e.g., de Prenter et al. [2018]; Griebel and Schweitzer [2003]). Similar estimates through generalized eigenvalue problems are also employed for variationally-consistent patch coupling (cf., e.g., Apostolatos et al. [2014]; Embar et al. [2010]; Hansbo [2005]; Harari and Grosu [2015]; Hu et al. [2018]; Jiang et al. [2015]; Nguyena et al. [2013]; Ruess et al. [2014]).

5.1 The trimmed-domain Galerkin form

The finite-dimensional spaces for trimmed analysis can be defined using a fictitious domain Ω^{fict} containing the physical domain $\Omega \subset \Omega^{\text{fict}}$. The domain Ω^{fict} can be chosen of a shape that can be trivially meshed. For example in two dimensions, Ω^{fict} can be rectangular and discretized by a Cartesian grid of elements. A finite-dimensional subspace $\mathcal{W}^h(\Omega^{\text{fict}}) \subset \mathcal{H}^1(\Omega^{\text{fict}})$ is defined on such a mesh. For example, $\mathcal{W}^h(\Omega^{\text{fict}})$ can be spanned by a finite number of B-splines or piecewise polynomials defined on a parameter space $\hat{\Omega}^{\text{fict}}$ combined with the geometrical mapping $\Omega^{\text{fict}} = \boldsymbol{F}(\hat{\Omega}^{\text{fict}})$ (cf., e.g., Hughes [2000]; Hughes et al. [2005]). It is assumed that the functions in $\mathcal{W}^h(\Omega^{\text{fict}})$ have non-empty support on Ω, namely

$$\underline{\text{supp}}\left(w^h\right) \cap \Omega \neq \emptyset, \qquad \forall w^h \in \mathcal{W}^h(\Omega^{\text{fict}}). \tag{18}$$

A discrete space for Problem (w) can be defined as

$$\mathcal{W}^h(\Omega) = \underline{\text{span}}\left\{ w^h\big|_\Omega \,:\, w^h \in \mathcal{W}^h(\Omega^{\text{fict}}) \right\}. \tag{19}$$

The trimmed Galerkin form of Problem (w) can be formulated as

$$\begin{aligned} &\text{find } u^h \in \mathcal{W}^h(\Omega), \\ &\text{such that } a(w^h, u^h) + a_w(w^h, u^h) = l(w^h), \qquad \forall w^h \in \mathcal{W}^h(\Omega). \end{aligned} \tag{g}$$

Note that the bilinear and linear forms are still defined as in Equations (12) and (13). Specifically, the integrals are computed on the physical domain Ω and not on Ω^{fict}. However, from the implementation point of view, it can be convenient to express the integrals over Ω as integrals over Ω^{fict} through the domain-indicator function $\alpha : \Omega^{\text{fict}} \to [0, 1]$

$$\alpha(\boldsymbol{x}) = \begin{cases} 1 & \text{if } \boldsymbol{x} \in \Omega, \\ 0 & \text{otherwise.} \end{cases}$$

In particular, for u^h, $w^h \in \mathcal{W}^h(\Omega^{\text{fict}})$, it holds

$$\begin{aligned} a(w^h, u^h) &= (\nabla w^h, \boldsymbol{\kappa} \nabla u^h)_\Omega, && (20)\\ &= (\nabla w^h, (\alpha\, \boldsymbol{\kappa})\, \nabla u^h)_{\Omega^{\text{fict}}}, && (21)\\ l(w^h) &= (w^h, f)_\Omega + (w^h, h)_{\Gamma_h} && (22)\\ &= (w^h, \alpha\, f)_{\Omega^{\text{fict}}} + (w^h, h)_{\Gamma_h}, && (23) \end{aligned}$$

where the domain of $\boldsymbol{\kappa}$ and f can be extended onto Ω^{fict}. The domain-indicator function α penalizes the material outside the physical domain, recovering the physics of the problem. However, a discontinuity is introduced in the integrands, requiring non-standard integration rules to retain accuracy (cf., e.g., Abedian et al. [2013]; Breitenberger et al. [2015]; Hubrich et al. [2017]; Joulaian et al. [2016]; Kudela et al. [2015, 2016]; Marussig and Hughes [2018]; Müller et al. [2013]; Parvizian et al. [2007]; Rank et al. [2012]). See Marussig and Hughes [2018] for a comprehensive review.

6 Conservative reactions to strong boundary conditions

In this section, the traditional way to compute the reactions is interpreted as testing a weak problem with specific test functions. This point of view will allow generalizing the computation of the reactions to trimmed domains and to bases that do not form a partition of unity. This interpretation is inspired by Brezzi et al. [2001]; Hughes et al. [2000] and similar to the argumentation therein. However, in this work, the focus is on obtaining the (integrated) total reaction flux instead of a "pointwise" approximation of the normal flux by a function defined on the boundary.

A conservative way to compute the reactions can be derived by considering a problem compatible with the mixed problem in Equations (7)–(9). Namely, other than the temperature boundary condition $u = g$ on Γ_g, the compatible reaction flux r is assumed to exist and is prescribed on Γ_g. The flux r

is such that the condition $u = g$ is retained on Γ_g. The remaining data of the problem $\boldsymbol{\kappa}$, f, and h are unchanged. For elastic problems, this corresponds to prescribing the forces that would enforce the displacement conditions.

In particular, let us consider the following boundary-value problem with compatible conditions on Γ_g

$$-\nabla \cdot (\boldsymbol{\kappa} \nabla u) = f \qquad \text{in } \Omega, \tag{24}$$
$$u = g \qquad \text{on } \Gamma_g, \tag{25}$$
$$\boldsymbol{\kappa} \nabla u \cdot \boldsymbol{n} = r \qquad \text{on } \Gamma_g, \tag{26}$$
$$\boldsymbol{\kappa} \nabla u \cdot \boldsymbol{n} = h \qquad \text{on } \Gamma_h. \tag{27}$$

For simplicity, the data $\boldsymbol{\kappa}$, f, r, g, h, and the boundary $\partial\Omega$ are assumed to be "smooth enough" for the following manipulations to hold. Given a solution $u^* \in \mathcal{H}^2(\Omega)$ for the mixed problem of Equations (7)–(9), it will also be a solution for the problem of Equations (24)–(27) with $r = (\boldsymbol{\kappa} \nabla u^* \cdot \boldsymbol{n})|_{\Gamma_g}$. Indeed, u^* satisfies Equations (24), (25), and (27), as they are the same as Equations (7)–(9). Moreover, Equation (26) is trivially satisfied by the definition $r = (\boldsymbol{\kappa} \nabla u^* \cdot \boldsymbol{n})|_{\Gamma_g}$.

Following standard variational arguments, one can formulate a weak form by multiplying Equation (24) by a test function w belonging to a test space chosen to be $\mathcal{W} = \mathcal{H}^1(\Omega)$ and integrating over Ω. This yields the following weak form

$$\begin{aligned} &\text{find } u \in \mathcal{S}_{g,\Gamma_g}(\Omega), \\ &\text{such that } a(w, u) = l(w) + (w, r)_{\Gamma_g}, \qquad \forall w \in \mathcal{W} = \mathcal{H}^1(\Omega). \end{aligned} \tag{R}$$

Note that the test space consists of the whole $\mathcal{H}^1(\Omega)$ function space, not requiring the test functions to be zero on any part of the boundary. In particular, the boundedness of Ω ensures that the constant $w = 1$ belongs to the test space $\mathcal{W} = \mathcal{H}^1(\Omega)$. Testing Problem (R) with $w = 1$ assures global equilibrium

$$0 = \int_\Omega f \, \mathrm{d}\boldsymbol{x} + \int_{\Gamma_h} h \, \mathrm{d}\boldsymbol{x} + \int_{\Gamma_g} r \, \mathrm{d}\boldsymbol{x}. \tag{28}$$

A solution $u^* \in \mathcal{H}^2(\Omega)$ for the original weak Problem (W) will also solve the strong form in Equations (24)–(27) and the compatible Problem (R).

Moreover, since $\mathcal{W}_{0,\Gamma_g}(\Omega)$ is a closed subspace of $\mathcal{H}^1(\Omega)$, then $\mathcal{H}^1(\Omega)$ admits the direct-sum representation [Rudin, 1991; Salsa, 2016]

$$\mathcal{H}^1(\Omega) = \mathcal{W}_{0,\Gamma_g}(\Omega) \oplus \mathcal{W}_{0,\Gamma_g}(\Omega)^\perp.$$

Namely, each $w \in \mathcal{H}^1(\Omega)$ admits a (unique) representation $w_0 + w_g$, with $w_0 \in \mathcal{W}_{0,\Gamma_g}(\Omega)$ and $w_g \in \mathcal{W}_{0,\Gamma_g}(\Omega)^\perp$. Following Bazilevs and Hughes [2007]; Hughes [2000]; Hughes et al. [2000], the arbitrariness of $w_0 + w_g = w \in \mathcal{H}^1(\Omega)$ in Problem (R) implies the arbitrariness of w_0 and w_g, allowing to reformulate the problem as

$$\begin{aligned} &\text{find } u \in \mathcal{S}_{g,\Gamma_g}(\Omega) \\ &\text{such that } a(w_0, u) = l(w_0), \qquad \forall w_0 \in \mathcal{W}_{0,\Gamma_g}(\Omega), \quad \text{and} \end{aligned} \tag{29}$$
$$a(w_g, u) = l(w_g) + (w_g, r)_{\Gamma_g}, \qquad \forall w_g \in \mathcal{W}_{0,\Gamma_g}(\Omega)^\perp. \tag{30}$$

Equation (29) is precisely the original variational form for strong boundary conditions in Problem (W). Therefore, if the compatible weak Problem (R) has a solution, this will also be the solution of the original Problem (W). Assuming the latter problem to have a unique solution in $\mathcal{S}_{g,\Gamma_g}(\Omega)$, this will identify the solution to the former problem.

Consequently, given an appropriate reaction flux r that makes the variational form in Problem (R) compatible with the original weak form in Problem (W), the conventional way to compute the reactions for conforming meshes can be interpreted as testing the variational form in Problem (R) with appropriate test functions. The total flux computed in this way will naturally satisfy the equilibrium expression given by the variational form. Specifically,

1. given a solution $u^* \in \mathcal{S}_{g,\Gamma_g}(\Omega)$ for the original weak Problem (W),
2. assume that there exists an $r \in \mathcal{L}_2(\Gamma_g)$ such that the variational form in Problem (R) holds for $u = u^*$.
3. Then, the unknown total flux $\int_{\Gamma_g} r \, \mathrm{d}\Gamma$ is obtained by testing the compatible variational form in Problem (R) with a function $w_g \in \mathcal{H}^1$ such that $w_g|_{\Gamma_g} = 1$.
4. The obtained total flux $\int_{\Gamma_g} r \, \mathrm{d}\Gamma$ will be in global equilibrium with the other fluxes, as the compatible variational form in Problem (R) also holds for $w = 1 \in \mathcal{H}^1$, yielding the global equilibrium in the sense of Equation (28).

Indeed, inserting w_g in Problem (R) yields

$$\begin{aligned} \int_{\Gamma_g} r \, \mathrm{d}\Gamma &= (w_g, r)_{\Gamma_g} \\ &= a(w_g, u^*) - l(w_g), \end{aligned} \tag{31}$$

where the term $a(w_g, u^*) - l(w_g)$ can be evaluated for known w_g and u^*.

The test function w_g defines the linear functional $R_{w_g}(u)$ associated with the reactions and defined as

$$R_{w_g}(u) = a(w_g, u) - l(w_g). \tag{32}$$

Note that such a functional is defined not only when $r \in \mathcal{L}_2(\Gamma_g)$, but it is continuous for any $u \in \mathcal{H}^1(\Omega)$, and l belongs to $\mathcal{H}^1(\Omega)^*$, the dual space of $\mathcal{H}^1(\Omega)$.

Similarly, the reactions on multiple disjoint Dirichlet boundaries $\{\Gamma_g^i\}_{i=1\dots n_b}$, such that

$$\Gamma_g = \bigcup_{i=1}^{n_b} \Gamma_g^i, \tag{33}$$

can be computed by means of test functions w_g^i such that $w_g^i|_{\Gamma_g^i} = 1$, $w_g^i|_{\Gamma_g^j} = 0$ for $i \neq j$.

6.1 Reactions for the Galerkin form

Employing the classical nodal finite element method (cf., e.g., Bathe [2007]; Hughes [2000]; Hughes et al. [2000]; Strang [1973]), the space $\mathcal{W}^h_{0,\Gamma_g}(\Omega)$ in the Galerkin Problem (G) is commonly based on a discretization that partitions Ω into a finite number of elements $\{\Omega_e\}_{e=1..n_e}$

$$\overline{\Omega} = \bigcup_{e=1}^{n_e} \overline{\Omega}_e.$$

Following Hughes [2000]; Hughes et al. [2000], let $\eta = \{1, 2, \dots, n_d\}$ be the set of indices of the associated nodes $\mathcal{N} = \{\boldsymbol{x}_A\}_{A\in\eta} \subset \overline{\Omega}$ and $\eta_g = \{A : \boldsymbol{x}_A \in \Gamma_g\} \subset \eta$ be the subset containing indices of nodes lying on Γ_g. Given the linear-independent nodal shape functions $\{N_A\}_{A\in\eta}$, where N_A is associated with node $\boldsymbol{x}_A$, the space spanned by $\{N_A\}_{A\in\eta}$ admits the direct-sum decomposition

$$\mathrm{span}\{N_A\}_{A\in\eta} = \underbrace{\mathrm{span}\{N_A\}_{A\in\eta\setminus\eta_g}}_{\mathcal{W}^h_{0,\Gamma_g}(\Omega)} \oplus \mathrm{span}\{N_A\}_{A\in\eta_g}. \tag{34}$$

The functions $\{N_A\}_{A\in\eta\setminus\eta_g}$ are a basis for the space $\mathcal{W}^h_{0,\Gamma_g}(\Omega)$, while $\{N_A\}_{A\in\eta_g}$ are commonly used to define g^h

$$g^h = \sum_{A\in\eta_g} g^h_A N_A. \tag{35}$$

The discrete linear system of equations takes the form

$$\boldsymbol{K}\boldsymbol{d} = \boldsymbol{F}, \tag{36}$$

where

$$\begin{aligned} K_{AB} &= a(N_A, N_B), & A, B &\in \eta, \\ F_A &= l(N_A), & A &\in \eta. \end{aligned}$$

Equation (36) can be partitioned into the blocks associated with the nodes identified by $\eta \setminus \eta_g$ and η_g

$$\left[\begin{array}{c|c} \boldsymbol{K}_{00} & \boldsymbol{K}_{0g} \\ \hline \boldsymbol{K}_{0g}^{\top} & \boldsymbol{K}_{gg} \end{array}\right] \left[\begin{array}{c} \boldsymbol{d}_0 \\ \hline \boldsymbol{d}_g \end{array}\right] = \left[\begin{array}{c} \boldsymbol{F}_0 \\ \hline \boldsymbol{F}_g \end{array}\right],$$

where

$$\begin{aligned} [\boldsymbol{K}_{00}]_{AB} &= a(N_A, N_B), & A, B &\in \eta \setminus \eta_g, \\ [\boldsymbol{K}_{0g}]_{AB} &= a(N_A, N_B), & A &\in \eta \setminus \eta_g, B \in \eta_g, \\ [\boldsymbol{K}_{gg}]_{AB} &= a(N_A, N_B), & A, B &\in \eta_g. \end{aligned}$$

The upper blocks yield the traditional problem for $\boldsymbol{d}_0$ with strong boundary conditions corresponding to Problem (G)

$$\boldsymbol{K}_{00}\boldsymbol{d}_0 = \boldsymbol{F}_0 - \boldsymbol{K}_{0g}\boldsymbol{d}_g. \tag{37}$$

The lower blocks correspond to the nodal forces associated with the reactions.

The computation of the reactions viewed as testing the variational form as in Equation (31), corresponds in the discrete case to testing the Galerkin form in Problem (G) with a $w_g^h \in \operatorname{span}\{N_A\}_{A\in\eta_g}$ such that $w_g^h\big|_{\Gamma_g} = 1$. For the discrete matrix system of equations, this corresponds to a left-multiplication by a coefficient vector representing the coordinates of w_g^h in the basis $\{N_A\}_{A\in\eta_g}$. In the case of the considered nodal partition-of-unity basis $\{N_A\}$, this takes the form

$$\left[\begin{array}{c|c} 0\ldots0 & 1\ldots1 \end{array}\right] \left\{ \left[\begin{array}{c|c} \boldsymbol{K}_{00} & \boldsymbol{K}_{0g} \\ \hline \boldsymbol{K}_{0g}^{\top} & \boldsymbol{K}_{gg} \end{array}\right] \left[\begin{array}{c} \boldsymbol{d}_0 \\ \hline \boldsymbol{d}_g \end{array}\right] - \left[\begin{array}{c} \boldsymbol{F}_0 \\ \hline \boldsymbol{F}_g \end{array}\right] \right\} = \left[\begin{array}{c|c} 0\ldots0 & 1\ldots1 \end{array}\right] \left[\begin{array}{c} \boldsymbol{0} \\ \hline \boldsymbol{r} \end{array}\right], \tag{38}$$

where the top block vanishes, as $\boldsymbol{d}_0$ solves Equation (37), and $\boldsymbol{r}$ represents the nodal reactions. Similarly, given a boundary portion $\Gamma_0 \subset \Gamma_g$, if it is possible to construct a test function $w_{g,0}^h \in \operatorname{span}\{N_A\}_{A\in\eta_g}$ such that $w_{g,0}^h\big|_{\Gamma_0} = 1$ and $w_{g,0}^h\big|_{\Gamma_g\setminus\Gamma_0} = 0$, then the reaction can be obtained by multiplication with a vector composed of the coordinates $w_{g,0}^h$ in the basis $\{N_A\}_{A\in\eta_g}$. This corresponds to the traditional algorithm in Table 1, as summarized in Table 2.

Continuous	(Equation (31))	$a(w_g, u) - l(w_g)$
Discrete	(Equation (38))	$\left[\begin{array}{c\|c} 0\ldots0 & 1\ldots1 \end{array}\right] \left\{ \left[\begin{array}{c\|c} \boldsymbol{K}_{00} & \boldsymbol{K}_{0g} \\ \hline \boldsymbol{K}_{0g}^{\top} & \boldsymbol{K}_{gg} \end{array}\right] \left[\begin{array}{c} \boldsymbol{d}_0 \\ \hline \boldsymbol{d}_g \end{array}\right] - \left[\begin{array}{c} \boldsymbol{F}_0 \\ \hline \boldsymbol{F}_g \end{array}\right] \right\}$
Algorithm	(Table 1)	$\sum_{A\in\eta_g} \int_\Omega \nabla N_A \cdot \left(\boldsymbol{\kappa}\nabla u^h\right) - N_A f \,\mathrm{d}\Omega - \int_{\Gamma_h} N_A h \,\mathrm{d}\Gamma$

Table 2: Traditional algorithm to compute the reactions viewed as testing the weak and Galerkin form with a specific test function.

7 Conservative reactions for trimmed meshes

Interpreting the total reaction as testing the weak form with specific test functions serves as a basis to obtain total conservative reactions for trimmed meshes. In the case of weak boundary conditions, the test space in Problem (w) naturally consists of the whole $\mathcal{H}^1(\Omega)$, containing elements w such that $w|_{\Gamma_g} = 1$. Therefore, it is not necessary to consider a compatible problem including the reactions. Instead, motivated by the principle of virtual work in Problem (w), the weak boundary condition term represents the normal flux action on the test functions with trace on Γ_g. In particular, given a $w_g \in \mathcal{H}^1$ such that $w_g|_{\Gamma_g} = 1$, the total flux can be computed by evaluating either side of

$$a(w_g, u) - l(w_g) = -a_w(w_g, u). \tag{39}$$

Note that the total flux computed as in Equation (39) is in the form of the extraction expressions studied in Babuška and Miller [1984]. For the Nitsche's method in Equation (16), this is further supported by the fact that it is variationally consistent. Namely, assuming enough regularity, integrating by parts, and using the arbitrariness of the test functions, the original strong form in Equations (7)–(9) is recovered. Therefore, a weak solution $u^* \in \mathcal{H}^2$ for Problem (w), with the weak boundary-condition term as in Equation (16), will also solve both the compatible strong form in Equations (24)–(27) with $r = (\boldsymbol{\kappa}\nabla u^* \cdot \boldsymbol{n})|_{\Gamma_g}$ and the associated weak form in Problem (R). The reactions can be computed as in Equation (31).

For the penalty method [Babuška, 1973], the weak form in Problem (w), with the weak boundary-condition term as in Equation (14), corresponds to the following perturbed strong form

$$-\nabla \cdot (\boldsymbol{\kappa}\nabla u) = f \qquad \text{in } \Omega, \tag{40}$$

$$\boldsymbol{\kappa}\nabla u \cdot \boldsymbol{n} + \beta(u - g) = 0 \qquad \text{on } \Gamma_g, \tag{41}$$

$$\boldsymbol{\kappa}\nabla u \cdot \boldsymbol{n} = h \qquad \text{on } \Gamma_h. \tag{42}$$

From Equation (41), it follows that $(1, \boldsymbol{\kappa}\nabla u \cdot \boldsymbol{n})_{\Gamma_g} = -(1, \beta(u-g))_{\Gamma_g} = -a_\beta(w_g, u) = a(w_g, u) - l(w_g)$ is a natural approximation to the flux on Γ_g.

7.1 Reactions for the Galerkin form

In order to compute the total flux on a disjoint portion of the boundary $\Gamma_0 \subset \Gamma_g$ for partition-of-unity bases on trimmed domains, one strategy can be to define a function $w^h \in \mathcal{W}^h(\Omega)$ that is one in a neighborhood of Γ_0, and has zero trace on $\Gamma_g \setminus \Gamma_0$. In particular, the function w^h, such that $w^h\big|_{\Omega_e} = 1$ for each element Ω_e cut by Γ_0, will also be such that $w^h\big|_{\Gamma_0} = 1$, even for a complex boundary Γ_0 that cannot be interpolated exactly by the shape functions.

Algorithmically, the only necessary modification to the procedure in Table 1 is to sum the fluxes q_A associated with functions N_A with non-zero trace on Γ_0 and zero trace on $\Gamma_g \setminus \Gamma_0$. An example is shown in Figure 4, where standard reactions for nodal linear shape functions are visually compared to the trimmed-mesh reactions with linear and quadratic B-splines shape functions (cf. Hughes et al. [2005]). Note that in Figure 4c the first two columns of control points are needed to compute the reactions, as these are the linear functions with support on the constrained boundary. In Figure 4d the first three columns of control points have to be considered for computing the reaction, as the basis functions' support grows with the order. This procedure can be summarized as in Table 3.

8 Conservative reactions for bases not forming a partition of unity

Equations (31) and (39) are already in a general form, suitable for bases that do not form a partition of unity. Using the same ideas as in Section 7, the strategy is to define a test function w^h that is one on each

Given the shape functions $\{N_A\}$, let $\tilde{\eta}(\Gamma_0) = \{A : N_A|_{\Gamma_0} \neq 0\}$ be the set of indices of shape functions with non-zero trace on Γ_0. It is assumed $N_A|_{\Gamma_g \setminus \Gamma_0} = 0 \ \ \forall A \in \tilde{\eta}(\Gamma_0)$.

1. For each $A \in \tilde{\eta}(\Gamma_0)$, compute the discrete fluxes

$$q_A = \int_\Omega \nabla N_A \cdot \left(\boldsymbol{\kappa} \nabla u^h\right) \, \mathrm{d}\Omega, \qquad q_A^e = \int_\Omega N_A f \, \mathrm{d}\Omega - \int_{\Gamma_h} N_A h \, \mathrm{d}\Gamma.$$

2. The reaction r on Γ_0 is obtained by summing the fluxes of shape functions with non-zero trace on Γ_0

$$r = \sum_{A \in \tilde{\eta}(\Gamma_0)} q_A - q_A^e.$$

Table 3: Algorithm for computing the reactions on trimmed meshes with partition-of-unity shape functions.

Given the shape functions $\{N_A\}$, let $\tilde{\eta}(\Gamma_0) = \{A \,|\, N_A|_{\Gamma_0} \neq 0\}$ be the set of indices of shape functions with non-zero trace on Γ_0. It is assumed $N_A|_{\Gamma_g \setminus \Gamma_0} = 0 \ \ \forall A \in \tilde{\eta}(\Gamma_0)$. Let $\{c_A\} \subset \mathbb{R}$ be the coordinates of 1 in the basis $\{N_A\}$, as in Equation (43).

1. For each $A \in \tilde{\eta}(\Gamma_0)$, compute the discrete fluxes

$$q_A = \int_\Omega \nabla N_A \cdot \left(\boldsymbol{\kappa} \nabla u^h\right) \, \mathrm{d}\Omega, \qquad q_A^e = \int_\Omega N_A f \, \mathrm{d}\Omega - \int_{\Gamma_h} N_A h \, \mathrm{d}\Gamma$$

2. The reaction r on Γ_0 is obtained by a weighted sum of fluxes associated with shape functions with non-zero trace on Γ_0

$$r = \sum_{A \in \tilde{\eta}(\Gamma_0)} c_A \ (q_A - q_A^e).$$

Table 4: Algorithm for computing the reactions on trimmed meshes. The basis functions do not need to form a partition of unity.

cut element. With the reasonable assumption that the basis functions $\{N_A\}$ can represent constants, let $c_A \in \mathbb{R}$ be the coefficient associated with the shape function N_A, such that

$$\sum_A c_A N_A = 1 \qquad \text{on } \overline{\Omega}. \tag{43}$$

The computation of the reactions are summarized as in Table 4, where the sum in Table 3 is generalized to a weighted sum of fluxes associated with basis functions with non-zero trace on Γ_0. Note that for partition-of-unity bases, it holds $c_A = 1$ for any A. In this case, the procedure in Table 4 is the same as the one in Table 3.

8.1 Reactions for hierarchical B-splines

For hierarchical B-splines ($\mathcal{HB}$), the coefficients $\{c_A\}$ can be obtained by projecting onto the hierarchical mesh the coefficients representing the function one on the base level. Since the standard B-splines form a partition of unity [Piegl and Tiller, 1995], the base-level coefficients are all equal to one. Let $\boldsymbol{c}^e$ be the vector of coefficients $\{c_A\}$ associated with functions with support on the element Ω_e, then $\boldsymbol{c}^e$ can be obtained as follows

$$\boldsymbol{c}^e = \boldsymbol{C}^e \mathbf{1}, \tag{44}$$

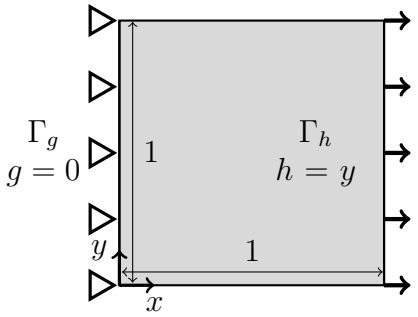

(a) Geometry description.

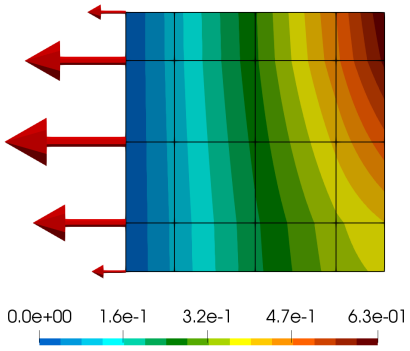

(b) Strong boundary conditions, linear elements.

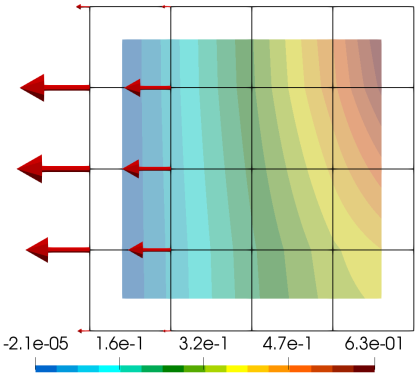

(c) Nitsche's method, linear elements, stabilization parameter $\gamma = 100$.

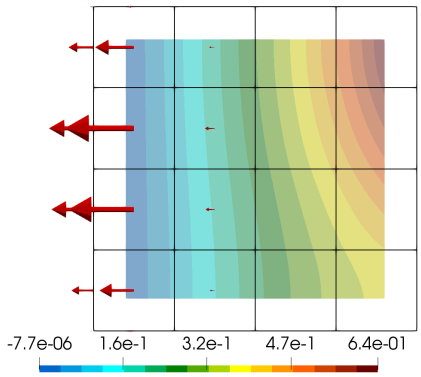

(d) Nitsche's method, quadratic B-splines, stabilization parameter $\gamma = 100$.

Figure 4: Solution field, mesh, and reactions for trimmed meshes. The reactions are depicted as red arrows in the x-direction located at the control points.

where $\mathbf{1}$ is a vector of ones and $\boldsymbol{C}^e$ is the element hierarchical extraction operator (see D'Angella et al. [2018]; Lorenzo et al. [2017]; Scott et al. [2014]). Algorithmically, this projection can be performed as described in D'Angella and Reali [2020]. See Figure 5a for an example of values for the coefficients $\{C_A\}$.

8.2 Reactions for integrated Legendre polynomials

The basis functions used in the p-version of the finite element method do not form a partition of unity. Given an order p, such a univariate basis is defined in the interval $[-1, 1]$ as [Szabó and Babuška, 1991]

$$\hat{\xi}_1(r) = \frac{1}{2}(1 + r) \tag{45}$$

$$\hat{\xi}_2(r) = \frac{1}{2}(1 - r) \tag{46}$$

$$\hat{\xi}_i(r) = P_{i-1}(r) \qquad i = 2, 3, \dots, p + 1, \tag{47}$$

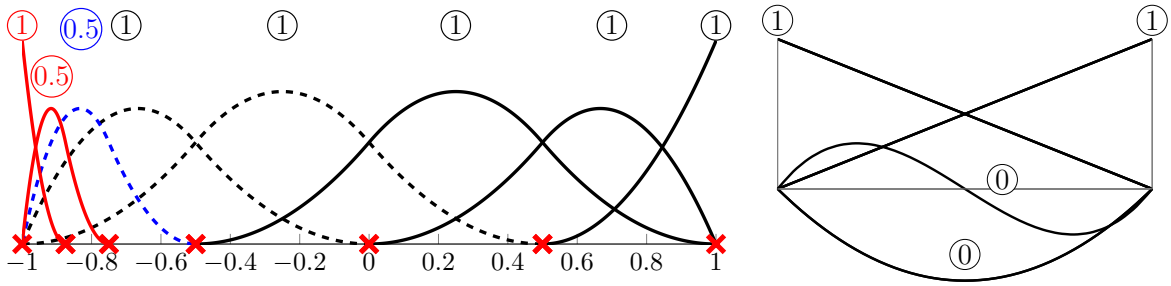

(a) Coefficients for a hierarchical B-spline basis ($\mathcal{HB}$).

(b) Coefficients for the integrated-Legendre basis [Szabó and Babuška, 1991] of order $p = 3$.

Figure 5: Example of coefficients (circled numbers) for computing the reactions with bases that do not form a partition of unity.

where $\hat{\xi}_1(r)$ and $\hat{\xi}_2(r)$ are the classical linear shape functions, while P_{i-1} is defined by an integral expression of the Legendre polynomials L_i

$$P_i(r) = \sqrt{\frac{2i-1}{2}} \int_{-1}^{r} L_{i-1}(t)\,\mathrm{d}t = \frac{1}{\sqrt{4i-2}} \left(L_i(r) - L_{i-2}(r)\right) \qquad i = 2, 3, \dots \ .$$

Since the linear shape functions form a partition of unity $\hat{\xi}_1 + \hat{\xi}_2 = 1$ on $[-1, 1]$, the remaining high-order functions $\hat{\xi}_i$, $i \geq 3$, will have a zero coefficient. See Figure 5b for an example. Similarly, for a basis obtained by the tensor product of the univariate basis in Equations (45)–(47), the coefficients will be the tensor product of the univariate coefficients. Namely, the linear shape functions will have coefficient one, while the remaining high-order functions will have a zero coefficient. In the case of a boundary-conforming mesh, this section agrees with the extraction of nodal forces presented in Babuška and Miller [1984]; Szabó and Babuška [2011]. However, this result is also valid for the more general case of trimmed meshes.

9 2D benchmark

In this section, a smooth problem involving a flux induced by a temperature difference on a curved geometry is considered. In two dimensions, a simple benchmark can be formulated on a quarter of annulus Ω with inner and outer radii r_1 and r_2, respectively (cf. Figure 6a). In particular, let us consider

$$\begin{aligned}
-\nabla \cdot (\boldsymbol{\kappa}\, \nabla u) &= 0 && \text{in } \Omega = \left\{\boldsymbol{x} \in (0, r_2)^2 : r_1 < \|\boldsymbol{x}\| < r_2\right\}, \\
u &= 2 \ln (r_1) && \text{on } \Gamma_0 = \{\boldsymbol{x} \in \partial\Omega : \|\boldsymbol{x}\| = r_1\}, \\
u &= 2 \ln (r_2) && \text{on } \Gamma_1 = \{\boldsymbol{x} \in \partial\Omega : \|\boldsymbol{x}\| = r_2\}, \\
\boldsymbol{\kappa}\, \nabla u \cdot \boldsymbol{n} &= 0 && \text{on } \partial\Omega \setminus (\overline{\Gamma_0 \cup \Gamma_1}),
\end{aligned}$$

where $\boldsymbol{\kappa}$ is the identity matrix. The analytical solution of the problem is the harmonic function (cf. Figures 6b and 6c)

$$u = 2 \ln \|\boldsymbol{x}\|.$$

Note that the data of the problem do not specify any external flux. The global equilibrium only assures that the flux across the Dirichlet boundary Γ_0 balances the flux across Γ_1. However, such total flux cannot be obtained directly from the source term or the boundary conditions.

The domain Ω is immersed in a Cartesian mesh of the bounding box $\Omega^{\text{fict}} = (0, r_2)^2$. One mesh example is shown in Figure 6d. The discontinuity in the integrands is resolved by reparameterized

integration-domains conforming to the physical domain Ω, as explained in Kudela et al. [2015, 2016]. The problem is solved with both Nitsche's and penalty methods, as in Equations (14) and (16), with parameters $\bar{\beta} = 10^2$ (cf. Equation (15)) and $\bar{\gamma} = 10(p+1)^2$ (cf. Equation (17)), similarly to Antolin et al. [2019]; Johansson et al. [2019]. The immersed B-splines analysis is compared to the solution obtained by a conforming NURBS mesh with similar element size h and strong Dirichlet boundary conditions.

The energy error of the numerical solution u^h is computed with respect to the bilinear form $a(\cdot,\cdot)$ of the original problem without weak boundary conditions. In particular, the error

$$e(u^h) = \sqrt{\frac{1}{2}\, a(u-u^h, u-u^h)} \tag{48}$$

for the conforming mesh is shown in Figure 7a to have a similar convergence behavior for both Nitsche's and penalty methods. The conservative fluxes q_0^c, q_1^c are computed on the boundaries Γ_0 and Γ_1 according to Table 3. The direct fluxes are numerically integrated as follows

$$q_i^h = \int_{\Gamma_i} \boldsymbol{\kappa} \nabla u^h \cdot \boldsymbol{n} \, \mathrm{d}\Gamma, \qquad\qquad i \in \{0,1\}. \tag{49}$$

Figures 7c and 7d show the relative flux error

$$e_i(q) = \left| 1 - \frac{q}{\int_{\Gamma_i} \boldsymbol{\kappa} \nabla u \cdot \boldsymbol{n} \, \mathrm{d}\Gamma} \right|. \tag{50}$$

for both the direct fluxes $e_i(q^h)$ (dashed lines) and for the conservative ones $e_i(q^c)$ (solid lines). Note that the conservative reactions yield more accurate results than the direct approach and show an apparent convergence to the analytical total flux. Nitsche's method yields convergence rates that are two times higher than the strain-energy error rates, similar to those obtained with the conforming mesh (cf. Figures 7b and 7d). This phenomenon is often referred to as superconvergence [Babuška and Miller, 1984; Hughes et al., 2000; Szabó and Babuška, 2011; Wahlbin, 1995]. These rates of convergence are not attained by the penalty method, as shown in Figure 7c. Indeed, the penalty method accurately computes the reactions of a perturbed problem, and the penalty parameter is scaled with h^p. Instead, if the penalty parameter is scaled as $\beta = \bar{\beta}/h^{2p}$, the same rates of convergence as the conforming mesh and Nitsche's method are attained, as shown in Figure 8a.

The equilibrium error

$$e(q_0, q_1) = \left| 1 - \frac{q_0}{-q_1} \right| \tag{51}$$

is shown in Figure 8b for both direct fluxes $e(q_0^h, q_1^h)$ (dashed lines) and conservative fluxes $e(q_0^c, q_1^c)$ (solid lines). Note that the conservative fluxes are in equilibrium up to small numerical inaccuracies that grow as the condition number with order $O(h^{-2})$. The direct-flux equilibrium error is several orders of magnitude higher than the one for the conservative fluxes.

10 Façade element

The model problem for the façade element introduced in Section 2 is solved with trivariate B-splines. The obtained conservative reactions yield a total flux converging to the same value for both Nitsche's and penalty methods. This behavior does not seem to hold for the direct approach: compare Figures 9a and 9b to Figures 3a and 3c.

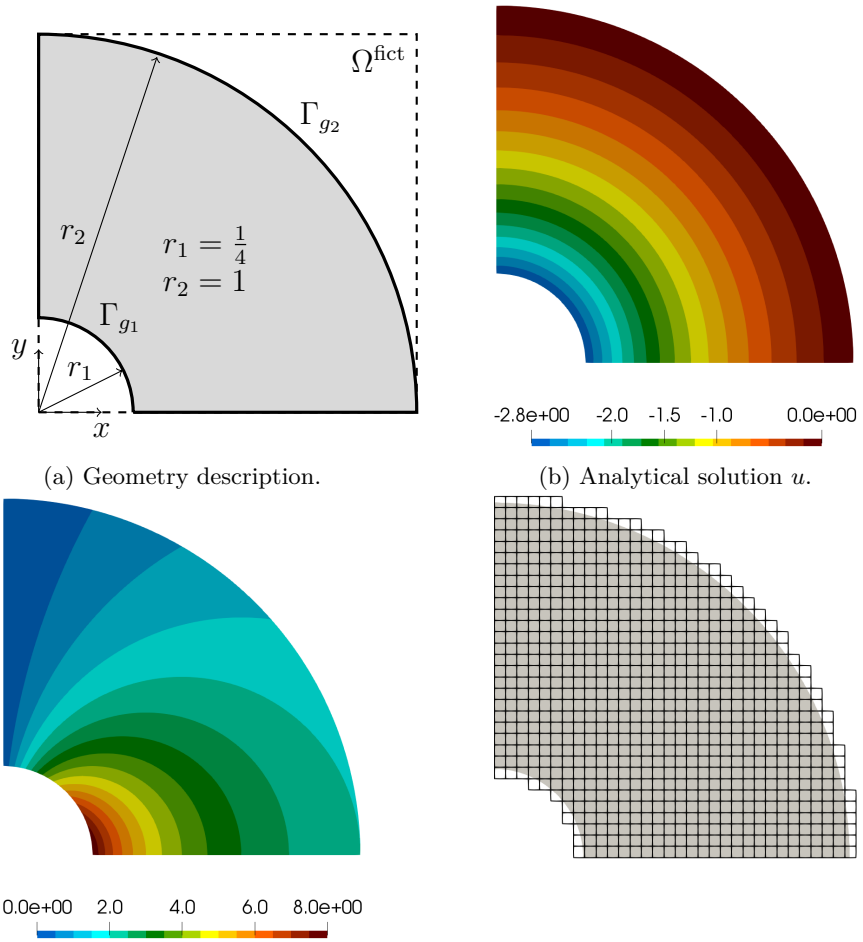

(a) Geometry description.

(b) Analytical solution u.

(c) x-component $u_{,x}$ of the analytical flux.

(d) Example of computational mesh.

Figure 6: 2D benchmark. Geometry, analytical solution, and mesh example.

11 Trimmed Kirchhoff-Love shell example

The presented reaction computation can be extended to the following weak form of the Kirchhoff-Love shell problem with weak boundary conditions (cf., e.g., Apostolatos et al. [2015]; Cirak [2006]; Coradello et al. [2020b]; Guo and Ruess [2015]; Herrema et al. [2019]; Kiendl et al. [2009])

$$\begin{aligned} &\text{find } \boldsymbol{u} \in \mathcal{H}^2(\Omega), \\ &\text{such that } a(\boldsymbol{w},\, \boldsymbol{u}) + b^{\text{disp}}(\boldsymbol{w}, \boldsymbol{u}) + b^{\text{rot}}(\boldsymbol{w}, \boldsymbol{u}) = l(\boldsymbol{w}), \qquad \forall \boldsymbol{w} \in \mathcal{H}^2(\Omega), \end{aligned} \tag{52}$$

where $a(\boldsymbol{w}, \boldsymbol{u})$ is the bilinear form representing the internal work

$$a(\boldsymbol{w}, \boldsymbol{u}) = \int_\Omega \boldsymbol{\varepsilon}(\boldsymbol{w}) \,:\, \boldsymbol{N}(\boldsymbol{u}) \,\mathrm{d}\Omega + \int_\Omega \boldsymbol{\kappa}(\boldsymbol{w}) \,:\, \boldsymbol{M}(\boldsymbol{u}) \,\mathrm{d}\Omega.$$

The symbols $\boldsymbol{\varepsilon}$ and $\boldsymbol{\kappa}$ denote the membrane and bending strain tensors, respectively, while $\boldsymbol{N}$ and $\boldsymbol{M}$ are the in-plane stress and bending moment. The term $l(\boldsymbol{w})$ is the linear functional representing the external work of a volumetric body load $\boldsymbol{f}$ and the traction $\boldsymbol{t}$ over the boundary $\Gamma_t \subset \partial\Omega$

$$l(\boldsymbol{w}) = \int_\Omega \boldsymbol{w} \cdot \boldsymbol{f} \,\mathrm{d}\Omega + \int_{\Gamma_t} \boldsymbol{w} \cdot \boldsymbol{t} \,\mathrm{d}\Gamma.$$

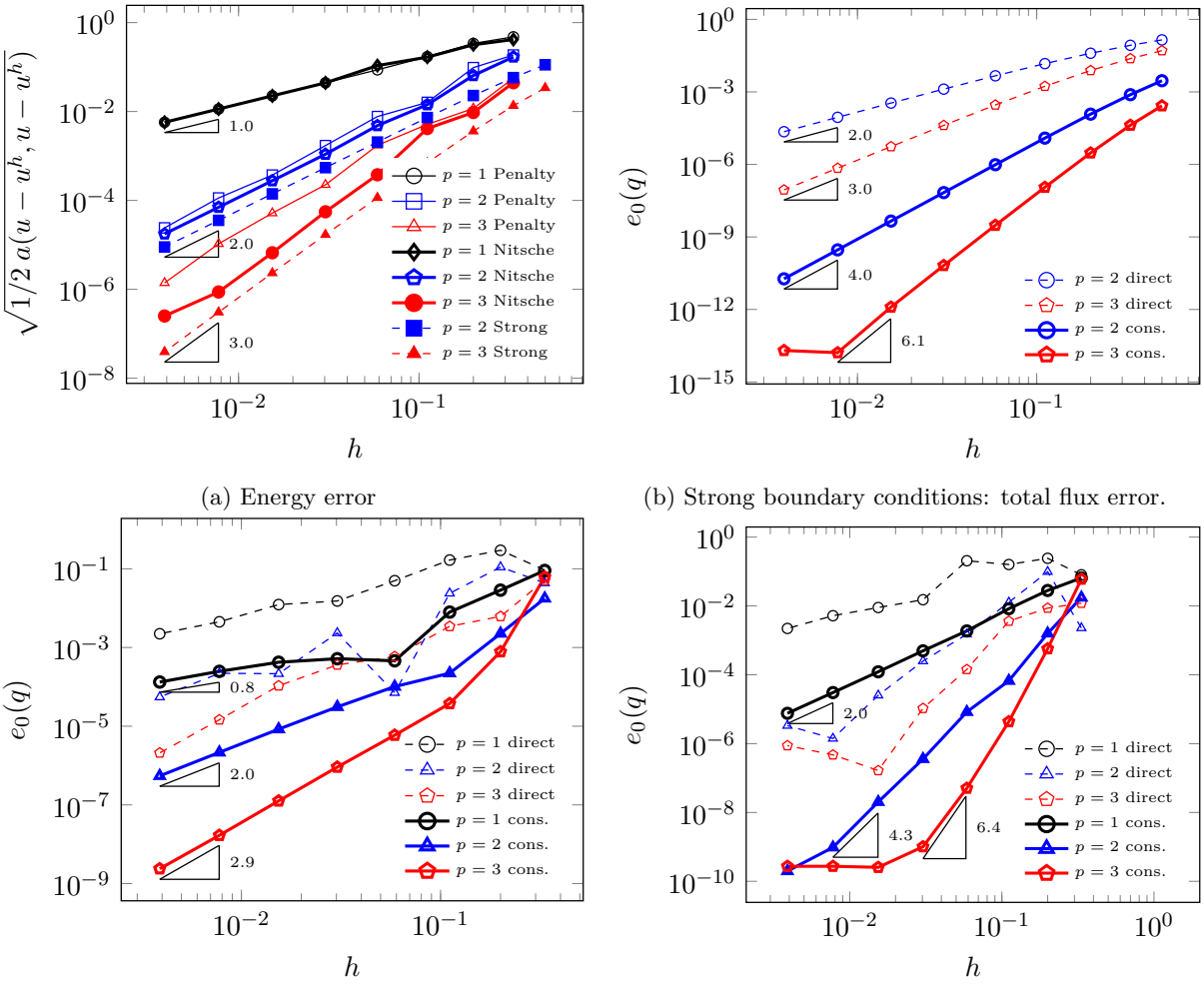

(a) Energy error

(b) Strong boundary conditions: total flux error.

(c) Penalty method: total flux error.

(d) Nitsche's method: total flux error.

Figure 7: 2D benchmark. Energy error and flux errors for direct fluxes (dashed lines) and conservative fluxes (solid lines).

For simplicity, only zero external bending moments are considered. The term $b^{\text{disp}}(\boldsymbol{w}, \boldsymbol{u})$ penalizes a displacement different than $\boldsymbol{g}$ on the boundary $\Gamma_g \subset \partial\Omega$

$$b^{\text{disp}}(\boldsymbol{w}, \boldsymbol{u}) = \int_{\Gamma_g} \beta^{\text{disp}}\, \boldsymbol{w} \cdot (\boldsymbol{u} - \boldsymbol{g})\, \mathrm{d}\Gamma,$$

where $\beta^{\text{disp}} \in \mathbb{R}$ is a user-defined penalty parameter. Finally, the term $b^{\text{rot}}(\boldsymbol{w}, \boldsymbol{u})$ penalizes the normal rotations on the boundary $\Gamma_\theta \subset \partial\Omega$

$$b^{\text{rot}}(\boldsymbol{w}, \boldsymbol{u}) = \int_{\Gamma_\theta} \beta^{\text{rot}}\, (\boldsymbol{n} \cdot \boldsymbol{\Phi}(\boldsymbol{w}))\, (\boldsymbol{\Phi}(\boldsymbol{u}) \cdot \boldsymbol{n})\, \mathrm{d}\Gamma,$$

where $\beta^{\text{rot}} \in \mathbb{R}$ is a user-defined penalty parameter, the symbol $\boldsymbol{n}$ represents the outward in-plane normal to the boundary Γ_θ, and $\boldsymbol{\Phi}(\boldsymbol{u}) = \boldsymbol{a}_3(\boldsymbol{u}) - \boldsymbol{A}_3$ denotes the angle between the shell normal in its undeformed $\boldsymbol{A}_3$ configuration and deformed $\boldsymbol{a}_3(\boldsymbol{u})$ configuration after applying the deformation $\boldsymbol{u}$. See Guo and Ruess [2015]; Herrema et al. [2019] for a detailed review. Following Herrema et al. [2019], given the Young's modulus E, the Poisson's ratio ν, the thickness t, and the size h of the smallest element, the penalty

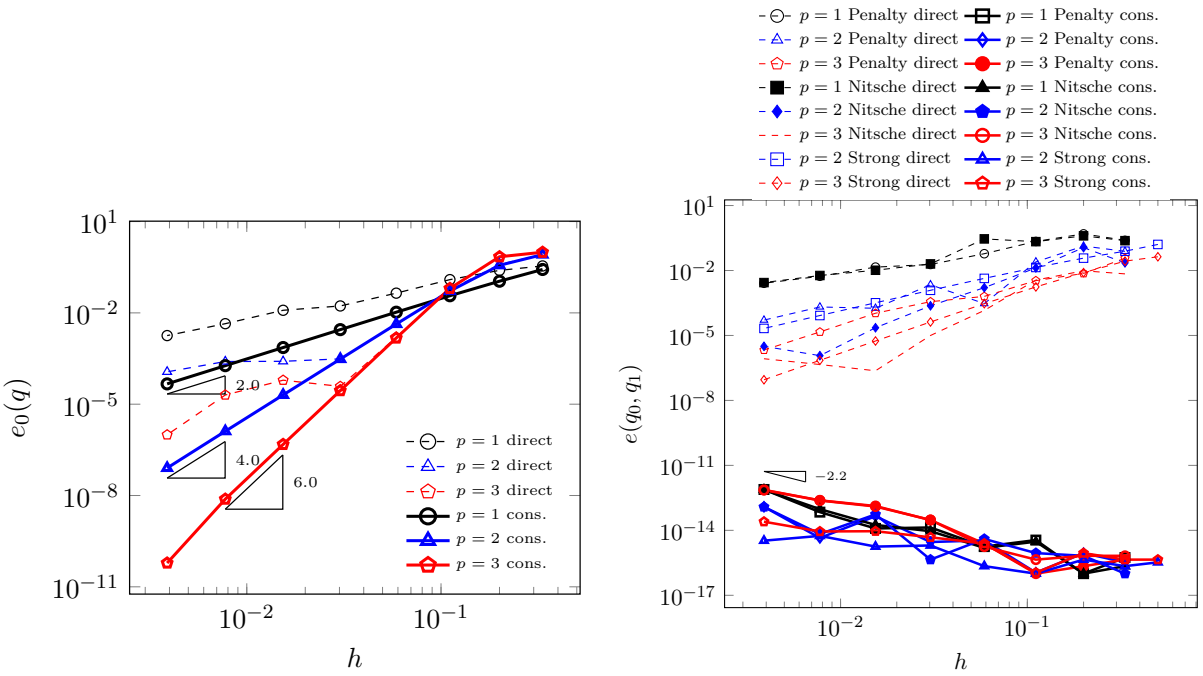

(a) Penalty method: total flux error with penalty parameter $\beta = \bar{\beta}/h^{2p}$.

(b) Equilibrium error of direct fluxes (dashed lines) and conservative fluxes (solid lines). The conservative fluxes (lines below) are in equilibrium up to machine precision.

Figure 8: 2D benchmark. Equilibrium error and improved convergence in the flux error obtained by the penalty method.

parameters are scaled as

$$\beta^{\text{disp}} = \bar{\beta}\frac{Et}{h(1-\nu^2)}$$
$$\beta^{\text{rot}} = \bar{\beta}\frac{Et^3}{12h(1-\nu^2)},$$

where the common parameter $\bar{\beta} \in \mathbb{R}$ is user-defined. In the following, the value $\bar{\beta} = 10^3$ is used, since in Herrema et al. [2019] this value is shown to be suitable for various examples in the context of multi-patch penalty coupling.

Following the reasoning of the previous sections, the ith reaction component, r_i, corresponding to the traction on Γ_g is computed by testing the variational form with a test function $\boldsymbol{w}^{g,i} \in \mathcal{H}^2$ such that $w_i^{g,i}\big|_{\Gamma_g} = 1$, $w_j^{g,i}\big|_{\Gamma_g} = 0$ for $j \neq i$ and such that $(\Phi(\boldsymbol{w}^{g,i}) \cdot \boldsymbol{n})\big|_{\Gamma_\theta} = 0$. In particular, given a known displacement field $\boldsymbol{u}^* \in \mathcal{H}^2$, the ith component of the total reaction can be computed by evaluating either side of the following equation

$$a(\boldsymbol{w}^{g,i}, \boldsymbol{u}^*) - l(\boldsymbol{w}^{g,i}) = -b^{\text{disp}}(\boldsymbol{w}^{g,i}, \boldsymbol{u}^*). \tag{53}$$

The same strategy as in Sections 7 and 8 can be applied to the present case to evaluate the reactions on trimmed geometries with bases that do not form a partition of unity. The global equilibrium is confirmed in the example shown in Figure 10a. The edges of the circular hole on the left (blue curves) are clamped, while a traction $\boldsymbol{t} = (0, 0, 1)^\top$ is applied on the straight boundary marked in Figure 10a (red arrows).

The geometry is described by a B-spline patch stored in a STandard for the Exchange of Product model data (STEP) file format [ISO 10303-11:1994, 1994]. A (trimmed) computational mesh is obtained

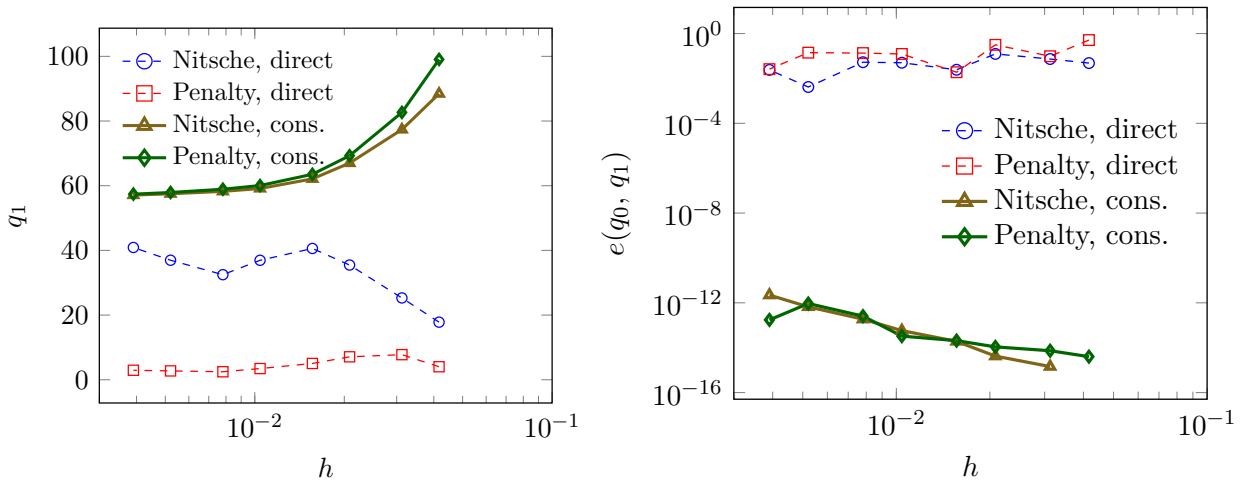

(a) Total flux.

(b) Equilibrium error.

Figure 9: Façade element example. Total flux and equilibrium error for the direct fluxes (dashed lines) and conservative fluxes (solid lines).

for numerical analysis by k-refinement on the geometric patch, as described in Cottrell et al. [2009]; Hughes et al. [2005]. The STEP file also contains the trimming curves in the parametric space of the B-spline patch, allowing to define accurate shell integration rules following Kudela et al. [2015], as explained in Coradello et al. [2020b]; Rank et al. [2011].

The problem is solved with an initial (trimmed) B-spline patch of uniform degree $p = 3$. The elements intersecting the physical domain Ω are shown in Figure 10a. Figure 10b shows the displacement magnitude on the deformed geometry. The problem is also solved with hierarchical B-splines [Forsey and Bartels, 1988; Vuong et al., 2011] with several refinement levels. The elements cut by the clamped boundary are recursively refined up to a refinement level l. Additionally, some elements totally outside the physical domain are refined to ensure that the finest-level hierarchical functions are activated, as explained in Coradello et al. [2020a]. Specifically, for each cut-element Ω_e marked for refinement, it is also marked for refinement each element $\tilde{\Omega}_e \in \Omega^{\text{fict}} \setminus \overline{\Omega}$ contained in the support of basis functions of element Ω_e. See Coradello et al. [2020a] for details. A graded mesh is obtained by enforcing a mesh-admissibility class equal to one [Bracco et al., 2019; Buffa and Giannelli, 2016]. Namely, each element can have active basis functions belonging to at most two consecutive levels. Details can be found in Bracco et al. [2019]; Buffa and Giannelli [2016]; Carraturo et al. [2019]. Figure 10c shows the mesh obtained after $l = 5$ recursive refinements, along with the von Mises stress around the clamped hole.

The basis functions having non-zero trace on the clamped edge belong to the hierarchical-refinement levels l and $l-1$. These functions do not form a partition of unity, and the reaction tractions are computed as described in Section 8.1. The mesh and discrete reactions for $l \in \{0, 2, 5\}$ are shown in Figures 10e–10g. Figure 10d shows the relative equilibrium error of the reaction traction $\boldsymbol{r}$ on the clamped edge with the applied external traction $\boldsymbol{t}$ computed as follows

$$e(\boldsymbol{r}, \boldsymbol{t}) = \frac{\|\boldsymbol{r} - \boldsymbol{t}\|_2}{\|\boldsymbol{t}\|_2}. \tag{54}$$

12 Conclusions

In this work, we formulated and investigated a conservative approach for computing reaction forces and fluxes based on the expression of global equilibrium given by the weak form. The discussed approach is suitable for trimmed meshes and non-interpolatory basis functions. We showed that the direct method

consisting of integrating the differentiated primal solution could perform particularly poorly for immersed methods. Instead, the conservative approach yields convergence rates two times higher than the energy-norm error for a two-dimensional benchmark with a smooth solution and weak boundary conditions. The approach is generalized to bases not forming a partition of unity, such as the hierarchical B-splines and the integrated Legendre polynomials.

In conclusion, this work aims at providing an accurate formulation for computing reaction forces and fluxes suitable for trimmed discretizations based on (locally-refined) non-interpolatory basis functions.

Acknowledgments

The authors Ernst Rank and Stefan Kollmannsberger gratefully acknowledge the support of the Deutsche Forschungsgemeinschaft (DFG, German Research Foundation) – Projektnummer 414265976 – TRR 277. Alessandro Reali gratefully acknowledges the support of the Italian Ministry of University and Research (MIUR) through the PRIN project XFAST-SIMS (No. 20173C478N).

References

Abedian, A., Parvizian, J., Düster, A., Khademyzadeh, H., and Rank, E. (2013). Performance of Different Integration Schemes in Facing Discontinuities in the Finite Cell Method. International Journal of Computational Methods, 10(03):1350002.

Akira, M. (1986). A mixed finite element method for boundary flux computation. Computer Methods in Applied Mechanics and Engineering, 57(2):239–243.

Antolin, P., Buffa, A., Puppi, R., and Wei, X. (2019). Overlapping multi-patch isogeometric method with minimal stabilization.

Apostolatos, A., Breitenberger, M., Wüchner, R., and Bletzinger, K.-U. (2015). Domain decomposition methods and Kirchhoff-Love shell multipatch coupling in isogeometric analysis. In Jüttler, B. and Simeon, B., editors, Isogeometric Analysis and Applications 2014, pages 73–101. Springer International Publishing.

Apostolatos, A., Schmidt, R., Wüchner, R., and Bletzinger, K.-U. (2014). A Nitsche-type formulation and comparison of the most common domain decomposition methods in isogeometric analysis. International Journal for Numerical Methods in Engineering, 97(7):473–504.

Babuška, I. (1973). The Finite Element Method with Penalty. Mathematics of Computation, 27(122):221–228.

Babuška, I. and Miller, A. (1984). The post-processing approach in the finite element methodpart 1: Calculation of displacements, stresses and other higher derivatives of the displacements. International Journal for Numerical Methods in Engineering, 20(6):1085–1109.

Barrett, J. W. and Elliott, C. M. (1987). Total flux estimates for a finite-element approximation of elliptic equations. IMA journal of numerical analysis, 7(2):129–148.

Bathe, K. J. (2007). Finite Element Procedures. Prentice Hall, New Jersey.

Bazilevs, Y., Hsu, M.-C., and Scott, M. (2012). Isogeometric fluid–structure interaction analysis with emphasis on non-matching discretizations, and with application to wind turbines. Computer Methods in Applied Mechanics and Engineering, 249-252:28–41. Higher Order Finite Element and Isogeometric Methods.

Bazilevs, Y. and Hughes, T. J. R. (2007). Weak imposition of Dirichlet boundary conditions in fluid mechanics. Computers & Fluids, 36(1):12–26.

Bracco, C., Buffa, A., Giannelli, C., and Vázquez, R. (2019). Adaptive isogeometric methods with hierarchical splines: An overview. Discrete & Continuous Dynamical Systems-A, 39(1):241.

Breitenberger, M., Apostolatos, A., Philipp, B., Wüchner, R., and Bletzinger, K. U. (2015). Analysis in computer aided design: Nonlinear isogeometric B-Rep analysis of shell structures. Computer Methods in Applied Mechanics and Engineering, 284:401–457.

Brezzi, F., Hughes, T. J. R., and Süli, E. (2001). Variational approximation of flux in conforming finite element methods for elliptic partial differential equations : a model problem. Atti della Accademia Nazionale dei Lincei. Classe di Scienze Fisiche, Matematiche e Naturali. Rendiconti Lincei. Matematica e Applicazioni, 12(3):159–166.

Buffa, A. and Giannelli, C. (2016). Adaptive isogeometric methods with hierarchical splines: Error estimator and convergence. Mathematical Models and Methods in Applied Sciences, 26(01):1–25.

Carey, G. (1982). Derivative calculation from finite element solutions. Computer Methods in Applied Mechanics and Engineering, 35(1):1–14.

Carey, G., Chow, S., and Seager, M. (1985). Approximate boundary-flux calculations. Computer Methods in Applied Mechanics and Engineering, 50(2):107–120.

Carraturo, M., Giannelli, C., Reali, A., and Vázquez, R. (2019). Suitably graded thb-spline refinement and coarsening: Towards an adaptive isogeometric analysis of additive manufacturing processes. Computer Methods in Applied Mechanics and Engineering, 348:660 – 679.

Cirak, F. (2006). Subdivision shells. In Motasoares, C. A., Martins, J. A. C., Rodrigues, H. C., Ambrósio, J. A. C., Pina, C. A. B., Motasoares, C. M., Pereira, E. B. R., and Folgado, J., editors, III European Conference on Computational Mechanics, pages 395–395, Dordrecht. Springer Netherlands.

Coradello, L., Antolin, P., Vázquez, R., and Buffa, A. (2020a). Adaptive isogeometric analysis on two-dimensional trimmed domains based on a hierarchical approach. Computer Methods in Applied Mechanics and Engineering, 364:112925.

Coradello, L., D'Angella, D., Carraturo, M., Kiendl, J., Kollmannsberger, S., Rank, E., and Reali, A. (2020b). Hierarchically refined isogeometric analysis of trimmed shells. Computational Mechanics, 66:431–447.

Cottrell, J. A., Hughes, T. J. R., and Bazilevs, Y. (2009). Isogeometric Analysis: Toward Integration of CAD and FEA. John Wiley & Sons.

D'Angella, D., Kollmannsberger, S., Rank, E., and Reali, A. (2018). Multi-level Bézier extraction for hierarchical local refinement of Isogeometric Analysis. Computer Methods in Applied Mechanics and Engineering, 328:147–174.

D'Angella, D. and Reali, A. (2020). Efficient extraction of hierarchical b-splines for local refinement and coarsening of isogeometric analysis. Computer Methods in Applied Mechanics and Engineering, 367:113131.

De Borst, R., Crisfield, M. A., Remmers, J. J., and Verhoosel, C. V. (2012). Nonlinear finite element analysis of solids and structures. John Wiley & Sons, second edition.

de Prenter, F., Lehrenfeld, C., and Massing, A. (2018). A note on the stability parameter in Nitsche,s method for unfitted boundary value problems. Computers & Mathematics with Applications, 75(12):4322 – 4336.

Düster, A., Rank, E., and Szabó, B. (2017). The p-Version of the Finite Element and Finite Cell Methods, pages 1–35. John Wiley & Sons.

Embar, A., Dolbow, J., and Harari, I. (2010). Imposing Dirichlet boundary conditions with Nitsche's method and spline-based finite elements. International Journal for Numerical Methods in Engineering, 83(7):877–898.

Forsey, D. R. and Bartels, R. H. (1988). Hierarchical B-spline Refinement. In Proceedings of the 15th Annual Conference on Computer Graphics and Interactive Techniques, SIGGRAPH '88, pages 205–212, New York, NY, USA. ACM.

Gresho, P. M., Lee, R. L., Sani, R. L., Maslanik, M. K., and Eaton, B. E. (1987). The consistent galerkin fem for computing derived boundary quantities in thermal and or fluids problems. International Journal for Numerical Methods in Fluids, 7(4):371–394.

Griebel, M. and Schweitzer, M. A. (2003). A Particle-Partition of Unity Method Part V: Boundary Conditions, pages 519–542. Springer Berlin Heidelberg, Berlin, Heidelberg.

Guo, Y. and Ruess, M. (2015). Weak dirichlet boundary conditions for trimmed thin isogeometric shells. Computers & Mathematics with Applications, 70(7):1425–1440. High-Order Finite Element and Isogeometric Methods.

Hansbo, P. (2005). Nitsche's method for interface problems in computational mechanics. GAMM-Mitteilungen, 28(2):183–206.

Harari, I. and Grosu, E. (2015). A unified approach for embedded boundary conditions for fourth-order elliptic problems. International Journal for Numerical Methods in Engineering, 104(7):655–675.

Herrema, A. J., Johnson, E. L., Proserpio, D., Wu, M. C., Kiendl, J., and Hsu, M.-C. (2019). Penalty coupling of non-matching isogeometric Kirchhoff-Love shell patches with application to composite wind turbine blades. Computer Methods in Applied Mechanics and Engineering, 346:810–840.

Hu, Q., Chouly, F., Hu, P., Cheng, G., and Bordas, S. P. (2018). Skew-symmetric nitsche's formulation in isogeometric analysis: Dirichlet and symmetry conditions, patch coupling and frictionless contact. Computer Methods in Applied Mechanics and Engineering, 341:188–220.

Hubrich, S., Stolfo, P. D., Kudela, L., Kollmannsberger, S., Rank, E., Schröder, A., and Düster, A. (2017). Numerical integration of discontinuous functions: Moment fitting and smart octree. Computational Mechanics, pages 1–19.

Hughes, T. J., Franca, L., Harari, I., Mallet, M., and Shakib, F. (1987). Finite element method for high-speed flows-consistent calculation of boundary flux. In 25th AIAA Aerospace Sciences Meeting, page 556.

Hughes, T. J. R. (2000). The Finite Element Method: Linear Static and Dynamic Finite Element Analysis. Dover Publications, Mineola, NY.

Hughes, T. J. R., Cottrell, J. A., and Bazilevs, Y. (2005). Isogeometric analysis: CAD, finite elements, NURBS, exact geometry and mesh refinement. Computer Methods in Applied Mechanics and Engineering, 194(39–41):4135–4195.

Hughes, T. J. R., Engel, G., Mazzei, L., and Larson, M. G. (2000). The continuous galerkin method is locally conservative. Journal of Computational Physics, 163(2):467 – 488.

ISO 10303-11:1994 (1994). Industrial automation systems and integration – Product data representation and exchange. Standard, International Organization for Standardization, Geneva, CH.

Jiang, W., Annavarapu, C., Dolbow, J. E., and Harari, I. (2015). A robust Nitsche's formulation for interface problems with spline-based finite elements. International Journal for Numerical Methods in Engineering, 104(7):676–696.

Johansson, A., Kehlet, B., Larson, M. G., and Logg, A. (2019). Multimesh finite element methods: Solving pdes on multiple intersecting meshes. Computer Methods in Applied Mechanics and Engineering, 343:672–689.

Joulaian, M., Hubrich, S., and Düster, A. (2016). Numerical integration of discontinuities on arbitrary domains based on moment fitting. Computational Mechanics, 57(6):979–999.

Kamensky, D., Evans, J. A., Hsu, M.-C., and Bazilevs, Y. (2017). Projection-based stabilization of interface lagrange multipliers in immersogeometric fluidthin structure interaction analysis, with application to heart valve modeling. Computers & Mathematics with Applications, 74(9):2068–2088. Advances in Mathematics of Finite Elements, honoring 90th birthday of Ivo Babuka.

Kamensky, D. M. (2016). Immersogeometric fluid–structure interaction analysis of bioprosthetic heart valves. PhD thesis, The University of Texas at Austin.

Kiendl, J., Bletzinger, K.-U., Linhard, J., and Wüchner, R. (2009). Isogeometric shell analysis with Kirchhoff-Love elements. Computer Methods in Applied Mechanics and Engineering, 198(49):3902 – 3914.

Kohnke, P. (2009). Theory reference for the mechanical apdl and mechanical applications. Ansys Inc, release, 12.

Kudela, L., Zander, N., Bog, T., Kollmannsberger, S., and Rank, E. (2015). Efficient and accurate numerical quadrature for immersed boundary methods. Advanced Modeling and Simulation in Engineering Sciences, 2(1):1–22.

Kudela, L., Zander, N., Kollmannsberger, S., and Rank, E. (2016). Smart octrees: Accurately integrating discontinuous functions in 3D. Computer Methods in Applied Mechanics and Engineering, 306:406–426.

Lorenzo, G., Scott, M. A., Tew, K., Hughes, T. J. R., and Gomez, H. (2017). Hierarchically refined and coarsened splines for moving interface problems, with particular application to phase-field models of prostate tumor growth. Computer Methods in Applied Mechanics and Engineering, 319:515–548.

Marussig, B. and Hughes, T. J. (2018). A review of trimming in isogeometric analysis: challenges, data exchange and simulation aspects. Archives of computational methods in engineering, 25(4):1059–1127.

Melbø, H. and Kvamsdal, T. (2003). Goal oriented error estimators for stokes equations based on variationally consistent postprocessing. Computer Methods in Applied Mechanics and Engineering, 192(5):613–633.

Müller, B., Kummer, F., and Oberlack, M. (2013). Highly accurate surface and volume integration on implicit domains by means of moment-fitting. International Journal for Numerical Methods in Engineering, 96(8):512–528.

Mungenast, M. (2017a). 3d-printed low-tech future facades - development of 3d-printed functional-geometries for building envelopes. In of Architecture, T. D. O. T. D. . F. and the Built Environment, editors, January 19th 2017 - Munich Powerskin Conference.

Mungenast, M. (2017b). Additive fertigung - anwendungsbeispiele für den modellbau. DER ENTWURF Deutsche BauZeitschrift.

Nguyena, V. P., Kerfriden, P., and Bordas, S. C. S. P. A. (2013). Nitsche's method method for mixed dimensional analysis: conforming and non-conforming continuum-beam and continuum-plate coupling.

Nitsche, J. (1971). Über ein Variationsprinzip zur Lösung von Dirichlet-Problemen bei Verwendung von Teilräumen, die keinen Randbedingungen unterworfen sind. Abhandlungen aus dem Mathematischen Seminar der Universität Hamburg, 36(1):9–15.

Oshima, M., Hughes, T. J., and Jansen, K. (1998). Consistent finite element calculations of boundary and internal fluxes. International Journal of Computational Fluid Dynamics, 9(3-4):227–235.

Parvizian, J., Düster, A., and Rank, E. (2007). Finite cell method. Computational Mechanics, 41(1):121–133.

Piegl, L. and Tiller, W. (1995). The NURBS Book. Monographs in Visual Communications. Springer Berlin Heidelberg, Berlin, Heidelberg.

Rank, E., Kollmannsberger, S., Sorger, C., and Düster, A. (2011). Shell Finite Cell Method: A high order fictitious domain approach for thin-walled structures. Computer Methods in Applied Mechanics and Engineering, 200(45-46):3200–3209.

Rank, E., Ruess, M., Kollmannsberger, S., Schillinger, D., and Düster, A. (2012). Geometric modeling, isogeometric analysis and the finite cell method. Computer Methods in Applied Mechanics and Engineering, 249-252:104–115.

Rudin, W. (1991). Functional analysis. McGraw-Hill Science, Engineering & Mathematics.

Ruess, M., Schillinger, D., Bazilevs, Y., Varduhn, V., and Rank, E. (2013). Weakly enforced essential boundary conditions for NURBS-embedded and trimmed NURBS geometries on the basis of the finite cell method. International Journal for Numerical Methods in Engineering, 95(10):811–846.

Ruess, M., Schillinger, D., Özcan, A. I., and Rank, E. (2014). Weak coupling for isogeometric analysis of non-matching and trimmed multi-patch geometries. Computer Methods in Applied Mechanics and Engineering, 269:46–71.

Salsa, S. (2016). Equazioni a derivate parziali: Metodi, modelli e applicazioni, volume 98. Springer.

Schillinger, D., Dedè, L., Scott, M. A., Evans, J. A., Borden, M. J., Rank, E., and Hughes, T. J. (2012a). An isogeometric design-through-analysis methodology based on adaptive hierarchical refinement of NURBS, immersed boundary methods, and T-spline CAD surfaces. Computer Methods in Applied Mechanics and Engineering, 249-252:116–150.

Schillinger, D., Ruess, M., Zander, N., Bazilevs, Y., Düster, A., and Rank, E. (2012b). Small and large deformation analysis with the p- and B-spline versions of the Finite Cell Method. Computational Mechanics, 50(4):445–478.

Scott, M., Thomas, D., and Evans, E. (2014). Isogeometric spline forests. Computer Methods in Applied Mechanics and Engineering, 269:222–264.

Siemens PLM Software Inc (2014). Nx nastran user's guide. https://docs.plm.automation.siemens.com/data_services/resources/nxnastran/10/help/en_US/tdocExt/pdf/User.pdf. Accessed: 15-4-2021.

Strang, G. (1973). An Analysis of the Finite Element Method. Prentice-Hall, Englewood Cliffs, N.J.

Szabó, B. A. and Babuška, I. (1991). Finite Element Analysis. John Wiley & Sons, New York.

Szabó, B. A. and Babuška, I. (2011). Introduction to Finite Element Analysis: Formulation, Verification, and Validation. Wiley, Chichester, West Sussex.

Utku, M. and Carey, G. (1982). Boundary penalty techniques. Computer Methods in Applied Mechanics and Engineering, 30(1):103–118.

van Brummelen, E. H., van der Zee, K. G., Garg, V. V., and Prudhomme, S. (2011). Flux Evaluation in Primal and Dual Boundary-Coupled Problems. Journal of Applied Mechanics, 79(1).

Vuong, A.-V., Giannelli, C., Jüttler, B., and Simeon, B. (2011). A hierarchical approach to adaptive local refinement in isogeometric analysis. Computer Methods in Applied Mechanics and Engineering, 200(49-52):3554–3567.

Wahlbin, L. (1995). Superconvergence in Galerkin Finite Element Methods. Springer, New York, 1995 edition.

Wu, M. C., Kamensky, D., Wang, C., Herrema, A. J., Xu, F., Pigazzini, M. S., Verma, A., Marsden, A. L., Bazilevs, Y., and Hsu, M.-C. (2017). Optimizing fluidstructure interaction systems with immersogeometric analysis and surrogate modeling: Application to a hydraulic arresting gear. Computer Methods in Applied Mechanics and Engineering, 316:668–693. Special Issue on Isogeometric Analysis: Progress and Challenges.

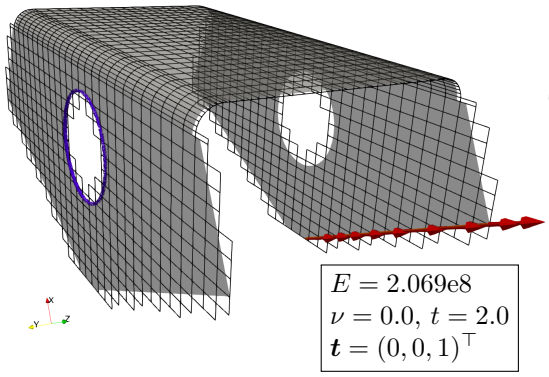

(a) Initial mesh, and boundary conditions: clamped edges (blue curves) and distributed traction (red arrows).

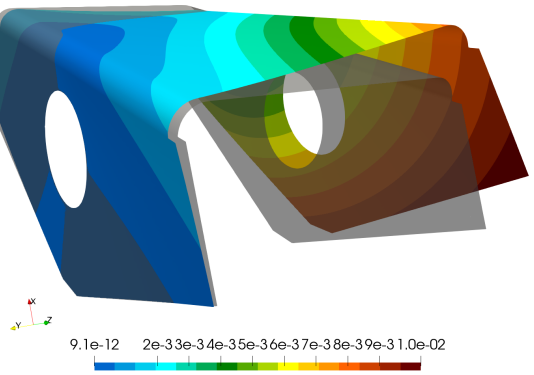

(b) Displacement magnitude.

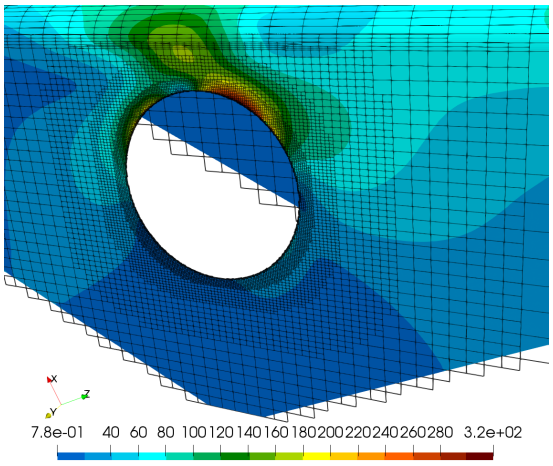

(c) Von Mises stress around clamped hole.

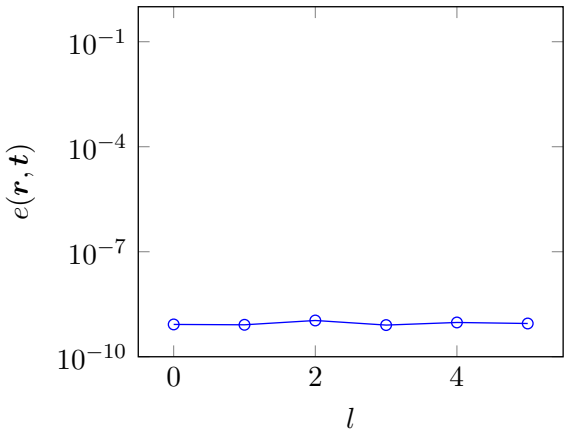

(d) Equilibrium error.

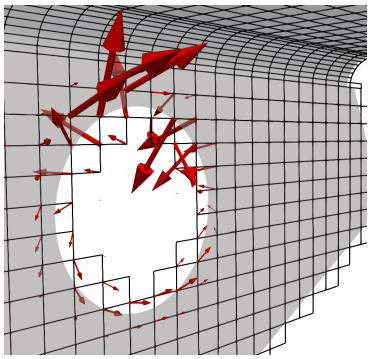

(e) Reaction tractions on initial mesh.

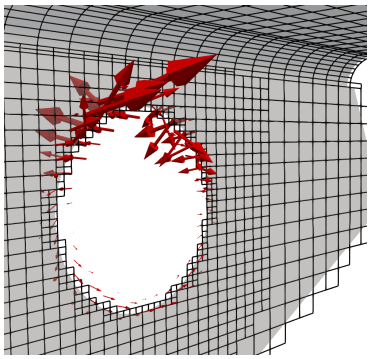

(f) Reaction tractions with 2 refinement levels.

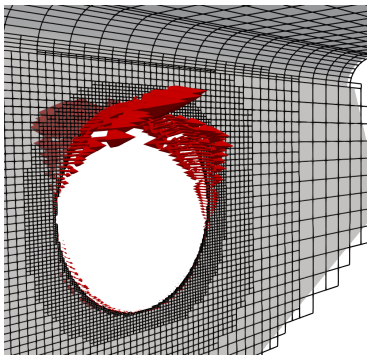

(g) Reaction tractions with 5 refinement levels.

Figure 10: Trimmed Kirchhoff-Love shell example.